3

ELECTRON BEAM INSTRUMENTS

3.0   INTRODUCTION

Whereas the previous chapter emphasizes imaging using microscopes, this chapter is concerned with analysis (compositional in particular) using fine electron probes, which provide fine spatial resolution. The beams used are either those in the SEM and TEM, discussed in the previous chapter (in which case the analytical techniques described here are used as adjuncts to the imaging capabilities of those instruments), or they involve electron beam columns specially constructed for an analytical mode. The Scanning Transmission Electron Microscope, STEM, and the Electron Microprobe, used for Electron Probe Microanalysis, EPMA, are two examples of the latter that are discussed in this chapter. A third example would be the Auger electron microprobe, used for scanning Auger Electron Spectroscopy, AES, but we choose to discuss this technique in Chapter 5 along with the other major electron spectroscopy methods, since all of them are primarily used to study true surface phenomena (monolayers), which is not generally the case for the techniques in this chapter.

The incoming electron beam interacts with the sample to produce a number of signals that are subsequently detectable and useful for analysis. They are X-ray emission, which can be detected either by Energy Dispersive Spectroscopy, EDS, or by Wavelength Dispersive Spectroscopy, WDS; visible or UV emission, which is known as Cathodoluminescence, CL; and Auger Electron Emission, which is the basis of Auger Electron Spectroscopy discussed in Chapter 5. Finally, the incoming

beam itself can lose discrete amounts of energy by inelastic collision, the values of which are determined by an electron energy analyzer. This is the basis of Electron Energy Loss Spectroscopy, EELS. Which of these classes of processes is more dominant, or more useful, depends on a number of factors, including the energy of the electron beam, the nature of the material (high or low Z), and the type of information sought (elemental composition, chemical composition, ultimate in spatial resolution, information limited to the surface, or information throughout the bulk by transmission measurement). A complete perspective for this can be obtained by comparing the articles in this section, plus the AES article, since they interrelate quite strongly. Some brief guidelines are given here.

All the methods, with the exception of CL, provide elemental composition. The most widely used is X-ray emission. If EDS is used the package can be quite inexpensive ($25,000 and up), and can be routinely fitted to SEMs, TEMs, and STEMs. In addition EDS is one of the two detection schemes in EPMA (the other is WDS). Its great advantage is its ability to routinely provide rapid multi element analysis for $Z>11$, with a detection limit of about 200 ppm for elements with resolved peaks. Its major disadvantages are very poor energy resolution, so that peaks are often overlapped; a detector problem that adversely affects detection limits; and the fact that the detector must remain cooled by liquid nitrogen or risk being destroyed. All these shortcomings of the EDS detector can be overcome by using the other detection scheme, WDS. The disadvantages of this scheme are that it is more expensive and cumbersome experimentally and does not have simultaneous multi element detection capability. For these reasons it is not so much used in conjunction with an SEM, TEM, or STEM, but is the heart of the *electron microprobe*, which is designed to combine WDS and EDS in the most effective analytical way.

The spatial resolution of X-ray emission does not usually depend on the diameter of the electron beam, since small beams spread out into a roughly pear-shaped "interaction volume" below the sample surface, and it is from this region that the X-ray signal is generated. This volume varies from a fraction of a micron to several microns depending on the electron beam energy (lower energy, smaller volume), and the material (lower Z, smaller volume). The exceptions are when the beam width is larger than a few microns, in which case it starts to dominate the resolution, or when the sample is very thin (hundreds of angstroms or less) so that the beam passes through before it can spread much. In this case the spatial resolution can be greatly improved toward that of the beam size itself. This is the case for thin samples in a TEM or STEM.

Cathodoluminescence, CL, involves emission in the UV and visible region and as such is not element specific, since the valence/conduction band electrons are involved in the process. It is therefore sensitive to electronic structure effects and is sensitive to defects, dopants, etc., in electronic materials. Its major use is to map out such regions spatially, using a photomultiplier to detect all emitted light without

spectral resolution in an SEM or STEM. Spatial resolution and depth resolution capabilities are, in principle, similar to X-ray emission, since the UV/visible emission comes from roughly the same interaction region. In practice lower electron beam energies are sometimes used in CL to improve spatial resolution.

EELS is used in a transmission mode in conjunction with TEMs and STEMs. Samples must be very thin (hundreds of angstroms) and beam energies must be high (100 keV and up) to prevent the single scattered EELS signal from being swamped by a multiple scattering background. A direct consequence of this requirement is that the spatial resolution of transmission EELS is not much worse than the beam size, since a 100-kV electron passing through a sample and scattered only once does not deviate much in direction. Thus, in a STEM with a 2-Å beam size the spatial resolution of EELS for a sample 100 Å thick might be only 3–4 Å! Although the main use of transmission EELS is to provide elemental composition like EDS/WDS it can also provide much information about chemical states and about electronic structure from the line shapes and exact positions of the energy loss peaks. EELS is also used in a reflection mode (REELS) in Auger spectrometers for surface analysis (see Chapter 5).

The STEM instrument itself can produce highly focused high-intensity beams down to 2 Å if a field-emission source is used. Such an instrument provides a higher spatial resolution compositional analysis than any other widely used technique, but to capitalize on this requires very thin samples, as stated above. EELS and EDS are the two composition techniques usually found on a STEM, but CL, and even AES are sometimes incorporated. In addition simultaneous crystallographic information can be provided by diffraction, as in the TEM, but with 100 times better spatial resolution. The combination of diffraction techniques and analysis techniques in a TEM or STEM is termed Analytical Electron Microscopy, AEM. A well-equipped analytical TEM or STEM costs well over $1,000,000.

Electron Probe Microanalysis, EPMA, as performed in an *electron microprobe* combines EDS and WDX to give quantitative compositional analysis in the reflection mode from solid surfaces together with the morphological imaging of SEM. The spatial resolution is restricted by the interaction volume below the surface, varying from about 0.2 μm to 5 μm. Flat samples are needed for the best quantitative accuracy. Compositional mapping over a 100×100 micron area can be done in 15 minutes for major components ($Z > 11$), several hours for minor components, and about 10 hours for trace elements.

3.1   EDS

Energy-Dispersive X-Ray Spectroscopy

ROY H. GEISS

Contents

- Introduction
- Principles of X-Ray Production
- Instrumentation
- Resolution, Peak Overlap, and Minimum Detection
- Sample Requirements
- Operational Considerations in Electron Microscopes
- Quantification
- Conclusions

Introduction

With modern detectors and electronics most Energy-Dispersive X-Ray Spectroscopy (EDS) systems can detect X rays from all the elements in the periodic table above beryllium, $Z = 4$, if present in sufficient quantity. The minimum detection limit (MDL) for elements with atomic numbers greater than $Z = 11$ is as low as 0.02% wt., if the peaks are isolated and the spectrum has a total of at least 2.5×10^5 counts. In practice, however, with EDS on an electron microscope, the MDL is about 0.1% wt. because of a high background count and broad peaks. Under conditions in which the peaks are severely overlapped, the MDL may be only 1–2% wt. For elements with $Z < 10$, the MDL is usually around 1–2% wt. under the best conditions, especially in electron-beam instruments.

The accuracy of quantitative analysis has been reported to be better than 2% relative for major concentrations, using well-polished standards having a composition similar to the sample. A more conservative figure of 4–5% relative should be expected for general analysis using pure element standards. For analysis without

using standards the accuracy will usually be much worse. The analysis of elements with concentrations less than 5% wt. will typically yield relative accuracies nearer 10%, even with standards. For samples with rough surfaces, such as fracture samples or small particles, the relative accuracy may be as bad as 50%.

Most applications of EDS are in electron column instruments like the scanning electron microscope (SEM), the electron probe microanalyzer (EPMA), and transmission electron microscopes (TEM). TEMs are further classified as conventional transmission (CTEM) or scanning transmission (STEM) instruments, depending on whether scanning is the primary imaging mode. A CTEM equipped with a scanning attachment and an EDS instrument is an Analytical Electron Microscope (AEM). X-ray spectrometers, with X-ray tube generators as sources and Si (Li) detectors have been used for both X-Ray Fluorescence Spectroscopy (XRF) and X-Ray Diffraction (XRD). Portable EDS systems also have been constructed using X-ray tube generators or radioactive sources.

A spectrum can be obtained from almost any sample, as long as it can be put on the specimen stage of the microscope. The choice of accelerating voltage should be determined by the type of sample one is studying, since the X-ray generation volume depends on the electron range in the material. In the study of thin films it is usually desirable to minimize the electron range and use an accelerating voltage E_0 just greater than E_c, the critical ionization voltage for the X-ray line of interest. For bulk samples it is more important to maximize X-ray production regardless of the electron range and, as will be discussed later, the accelerating voltage should be ideally 2–$2.5 \times E_c$. For example, consider the K-shell ionization of copper, for which $E_c = 8.98$ keV. To analyze a film only a few nm thick on a Si substrate, using the copper $K\alpha$, the accelerating voltage should be set near 10 keV. To analyze a bulk sample, more than a few μm thick, an accelerating voltage of 20–25 keV should be used.

With an MDL of 100–200 ppm for most elements, an EDS system is capable of detecting less than a monolayer of metal film on a substrate using $K\alpha$ lines at moderate accelerating voltages of 5–15 keV. Since many SEMs now have field emission electron guns providing high brightness probes at voltages of 2 keV and less, EDS analysis of even thinner films should be possible, at least in principle, since the electron range and hence, the generated X-ray volume will be very small. In this case, however, since all the X-ray lines will be low energy and in a small energy region, there may be many overlapped peaks that will have to be deconvoluted before quantitative analysis can be attempted. This deconvolution can be tricky, however, since the shape of the background in this energy range is difficult to model. In addition, the shape of the peaks in the low-energy region is often not Gaussian and the peak positions, especially for the K lines from low-Z elements, are often shifted.

Energy-dispersive X-ray spectroscopy has been used for quality control and test analysis in many industries including: computers, semiconductors, metals, cement, paper, and polymers. EDS has been used in medicine in the analysis of blood, tis-

sues, bones, and organs; in pollution control, for asbestos identification; in field studies including ore prospecting, archeology, and oceanography; for identification and forgery detection in the fine arts; and for forensic analysis in law enforcement. With a radioactive source, an EDS system is easily portable and can be used in the field more easily than most other spectroscopy techniques.

The main advantages of EDS are its speed of data collection; the detector's efficiency (both analytical and geometrical); the ease of use; its portability; and the relative ease of interfacing to existing equipment.

The disadvantages are: poor energy resolution of the peaks, (a typical EDS peak is about 100× the natural peak width, limited by the statistics of electron–hole pair production and electronic noise, which often leads to severe peak overlaps); a relatively low peak-to-background ratio in electron-beam instruments due to the high background coming from bremsstrahlung radiation emitted by electrons suffering deceleration on scattering by atoms; and a limit on the input signal rate because of pulse processing requirements.

Principles of X-Ray Production

X-rays are produced as a result of the ionization of an atom by high-energy radiation wherein an inner shell electron is removed. To return the ionized atom to its ground state, an electron from a higher energy outer shell fills the vacant inner shell and, in the process, releases an amount of energy equal to the potential energy difference between the two shells. This excess energy, which is unique for every atomic transition, will be emitted by the atom either as an X-ray photon or will be self-absorbed and emitted as an Auger electron. For example, if the K shell is ionized and the ejected K-shell electron is replaced by an electron from the L_3 shell, the emitted X ray is labeled a characteristic $K\alpha_1$ X ray. (See Figure 2 in the article on electron probe X-ray microanalysis). The hole that exists in the L shell will be filled by an electron from a higher shell, say the M shell, if one exists. This M–L transition may result in the emission of another X ray, labeled in turn according to one of the many M–L transitions possible. The cascade of transitions will continue until the last shell is reached. Thus, in an atom with many shells, many emissions can result from a single primary ionization.

Instrumentation

The heart of the energy-dispersive spectrometer is a diode made from a silicon crystal with lithium atoms diffused, or *drifted*, from one end into the matrix. The lithium atoms are used to compensate the relatively low concentration of grown-in impurity atoms by neutralizing them. In the diffusion process, the central core of the silicon will become intrinsic, but the end away from the lithium will remain p-type and the lithium end will be n-type. The result is a p-i-n diode. (Both lithium-
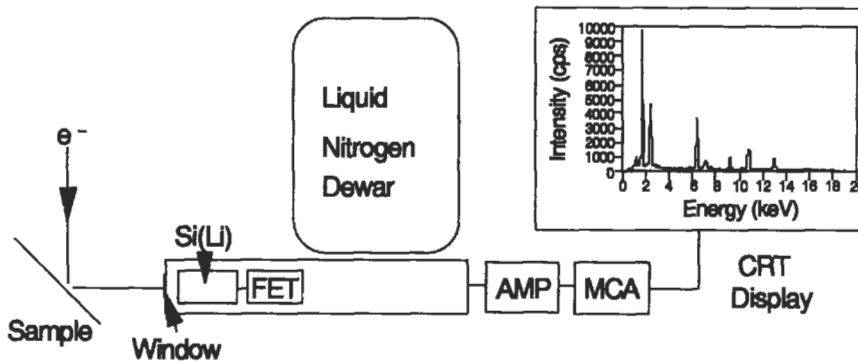
Figure 1 Schematic of an EDS system on an electron column. The incident electron interacts with the specimen with the emission of X rays. These X rays pass through the window protecting the Si (Li) and are absorbed by the detector crystal. The X-ray energy is transferred to the Si (Li) and processed into a digital signal that is displayed as a histogram of number of photons versus energy.

drifted and pure intrinsic germanium have been used as detectors, but much less frequently. These will be discussed later). A reverse bias electrical field of 100–1000 volts is applied to thin layers of gold evaporated onto the front and back surfaces of the diode.

When an X-ray photon enters the intrinsic region of the detector through the p-type end, there is a high probability that it will ionize a silicon atom through the photoelectric effect. This results in an X ray or an Auger electron, which in turn produces a number of electron–hole pairs in the Si (Li): one pair per 3.8 eV of energy. For example, a 6.4-keV X ray absorbed by the silicon atoms will produce about 1684 electron–hole pairs or a charge of about 2.7×10^{-13} Coulombs. Both charge carriers move freely through the lattice and are drawn to the detector contacts under the action of the applied bias field to produce a signal at the gate of a specially designed field effect transistor mounted directly behind the detector crystal. The transistor forms the input stage of a low-noise charge-sensitive preamplifier located on the detector housing. The output from the preamplifier is fed to the main amplifier, where the signal is finally amplified to a level that can be processed by the analog-to-digital converter (ADC) of the multichannel analyzer (MCA). See Figure 1. The height of the amplifier output pulse is proportional to the input preamplifier pulse, and hence is proportional to the X-ray energy.

For the amplifier pulse to be recognized in the ADC, it must exceed the lower level set by a discriminator, which is used to prevent noise pulses from jamming the converter. Once the pulse is accepted it is used to charge a capacitor that is discharged through a constant current source attached to an address clock typically
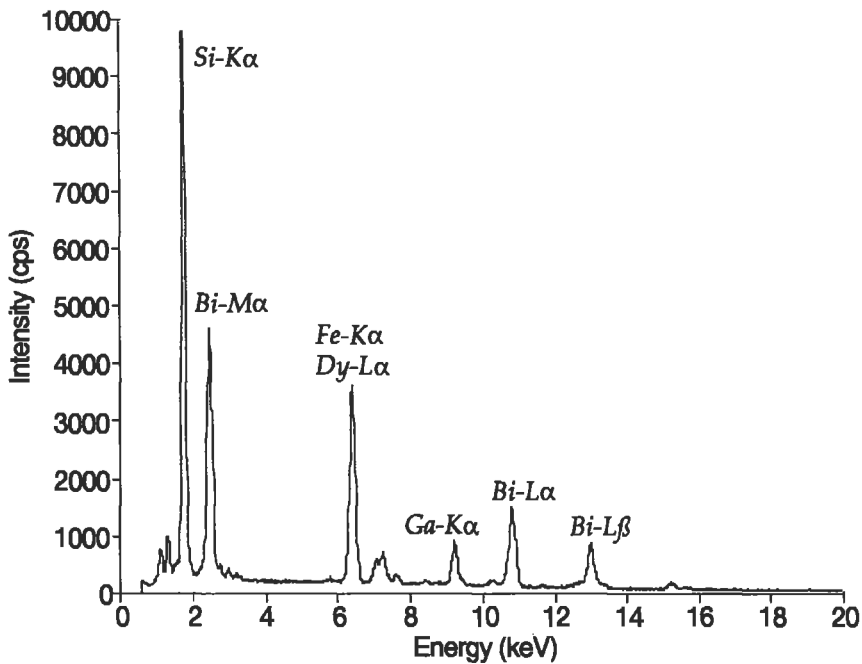
Figure 2 Standard output of an EDS spectrum. The horizontal axis is the energy scale is and the vertical axis is the number of photons per energy interval. The X-ray identification, element and line, is indicated in the vicinity of the peaks.

operating at 50 MHz. The time to discharge the capacitor to 0 V is proportional to the pulse amplitude, and hence to the X-ray energy. The 50-MHz clock produces a binary number in one of the 1024 channels typically used by the MCA in accordance with the time of the discharge, and increments the previously collected number in that channel by 1. By an energy calibration of the channels in the MCA, the collection of X-ray pulses may be displayed on a CRT as an energy histogram. A typical spectrum output from a thin alloy film using a TEM is shown in Figure 2.

To partition the incoming X rays into their proper energy channels, it is necessary to measure only single pulses. At high count rates, however, situations often arise where a second pulse reaches the main amplifier during the rise time of the preceding pulse. The two pulses may then combined into a single pulse whose energy is the combined energy of the two individual pulses. This process is known as pulse *pile-up* and the output, which is an artifact, is called a *sum peak*. Pile-up effects can be minimized with the use of electronic pulse rejection using a second pulse amplifier with a much faster response. Operationally, it is usually desirable to collect spectra with a dead time of less than 40%, or at an input count rate of about 5000 cps.

Detectors are maintained under vacuum at liquid nitrogen temperature to reduce electronic noise and to inhibit diffusion of the lithium when the bias voltage is applied. Most have a window covering the entrance to provide vacuum protection. The window in a standard detector is usually made from rolled beryllium foil, a few μm thick. Unfortunately, low-energy, or *soft*, X rays are strongly absorbed by the Be window, limiting the analysis range of these detectors to elements having atomic number $Z > 10$. To reduce the absorption, detectors are built either without windows at all or with windows made of new low-Z materials that can withstand atmospheric pressure. Detectors made with these low-Z windows show a marked increase in sensitivity to X rays from elements having $Z < 10$, compared to the Be window detectors.

Detector sensitivity drops off at the high-energy end (greater than 20 keV), where the Si (Li) crystal, which is typically 3–5 mm thick, becomes transparent to high-energy X rays. This may not be important in an SEM operated at 30 keV, since high-energy X rays will not be excited. But in a TEM operated at 100 keV or higher, the ability to detect hard X rays would be severely limited. In Figure 3, curves are plotted that show the detector's efficiency both at low energy, where the X-ray absorption of a standard Be window is compared to that of a low-Z window, and at high energy, where the high-energy drop-off is shown for the standard thickness Si (Li) crystals used today.

Spectrometers have been made using germanium crystals. The Ge crystals have been either lithium drifted, Ge (Li), or more recently, made from high-purity intrinsic germanium, HPGe. The HPGe crystal has the advantage that it can be allowed to warm to room temperature if it is not being used, saving the hassle of keeping the liquid nitrogen dewar filled. Germanium is much less transparent to high-energy electrons than silicon, because Ge ($Z = 32$) has a higher stopping power than Si ($Z = 14$), and should be able to detect very high energy X rays such as gold Kα, at 69 keV. This will be a distinct advantage when a TEM, operating at 100 keV and above and therefore capable of exciting high-energy X-ray lines, is used in the study of alloys containing elements that have severe peak overlap in the lower energy lines. However, germanium has some drawbacks; namely, a K-shell absorption edge at 11.1 keV, a complex L-shell absorption edge structure starting at 1.4 keV and a series of escape peaks in the range 2–12 keV. Thus, in the energy range 1–10 keV, the most frequently used range in EDS analysis, the detector is not as well behaved as Si (Li).

A major advantage of the energy-dispersive spectrometer is that it can be positioned very close to the sample and can present a large solid angle for the collection of emitted X rays. The solid angle in a typical EDS configuration is about 10 times greater than that of a WDS. With EDS, more X-ray photons will be collected per incident electron, so that either a smaller probe diameter or lower beam current can be used (which reduces specimen damage). Detectors are usually manufactured with an active area of either 10 mm^2 or 30 mm^2 diameter.
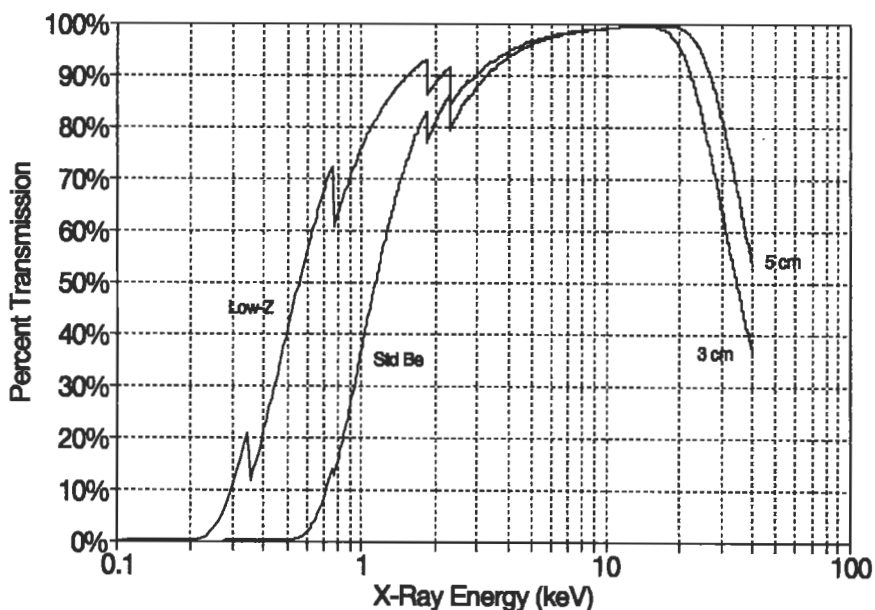
Figure 3   Curves showing the absorption of the window materials at low energy for a standard Be window and a low-Z window. The high-energy region shows the transmission of X rays through 3 mm and 5 mm thick Si (Li) crystals. Most detectors can be represented by a combination of one of the low-energy curves and one of the high-energy curves.

Since energy-dispersive spectrometers consist mostly of electronic components, they are easy to interface to most instruments. The only limitations are the need for a large liquid nitrogen cryostat to cool the spectrometer and high vacuum for the windowless detectors. Some Si (Li) detectors use mechanical cooling, called *Peltier* cooling, instead of the liquid nitrogen; this eliminates the large cryostat and the nagging requirement to keep it full. Unfortunately, the temperature reached with Peltier refrigerators is not as low as that obtained with liquid nitrogen, and the detector resolution suffers.

Most EDS systems are controlled by minicomputers or microcomputers and are easy to use for the basic operations of spectrum collection and peak identification, even for the computer illiterate. However, the use of advanced analysis techniques, including deconvolution of overlapped peaks, background subtraction, and quantitative analysis will require some extra training, which usually is provided at installation or available at special schools.

Resolution, Peak Overlap, and Minimum Detection

The energy resolution of a solid state detector is defined as the full width at half maximum (FWHM) of the peak obtained at energy E_0 when a monoenergetic beam of X rays having energy E_0 is incident on the detector. Ideally this width would be very small; but due to the statistical nature in the collection process of the electron–hole pairs, there will be some fluctuation in the measured energy of the X rays. For a modern energy-dispersive spectrometer, the FWHM of the peaks ranges from about 70 eV for the C $K\alpha$ at 0.282 keV to about 150 eV for the Cu $K\alpha$ at 8.04 keV. Improvements in detector resolution have focused on reducing the electronic noise contribution by improving the FET design and by using nonoptical charge restoration. Noise resolution as low as 40 eV has been achieved, giving a detector resolution of 128 eV FWHM at 5.89 keV.

Peak overlap, which follows from the poor resolution of the detector, is one of the major problems in EDS. For example, severe peak overlap occurs when two peaks of about the same amplitude are separated by less than half of the FWHM of the peaks. In this instance they will merge together and appear as one Gaussian peak. Unfortunately, in X-ray spectroscopy the peaks of the characteristic lines are often closer together then the resolution of the best EDS systems, and significant peak overlap follows. This presents problems not only with the identification of the individual peaks, but also with the determination of the amplitudes of the peaks for quantification. Improvements in detector resolution will obviously provide some relief to the problem, but even for the most optimistic resolution specification, there will still be many instances of peak overlap. An example of this is shown for the $BaTiO_3$ system in Figure 4, where the spectrum from a standard EDS is compared to that obtainable with a standard WDS using a LiF crystal; in the latter case the FWHM of the peaks is only a few eV. Peak overlap presents a particularly difficult problem in the analysis of soft X rays, especially when the K-line X rays from elements with $Z < 10$, the L-line X rays from transition metals or the M-line X rays from the rare earths are present. As previously mentioned, the resolution of most EDS detectors is about 60–90 eV in this region, which ranges from 300 to 1000 eV. To compound the problem, the peak shape is usually not purely Gaussian in this region, making computer deconvolution even more difficult. Here again, the resolution of a wavelength spectrometer will be only 5–10 eV, so that with the proper choice of analyzing crystal, peak overlap will not be a problem.

The minimum detection limit, MDL, of an isolated peak on a uniform background is proportional to the square root of the FWHM. So a 20% reduction in spectrometer resolution will produce about a 10% improvement in MDL. If there is peak overlap, however, then it can be shown that a 20% improvement in resolution can reduce the interference between overlapping peaks by a factor of 3, which gives about a 50% improvement in MDL.
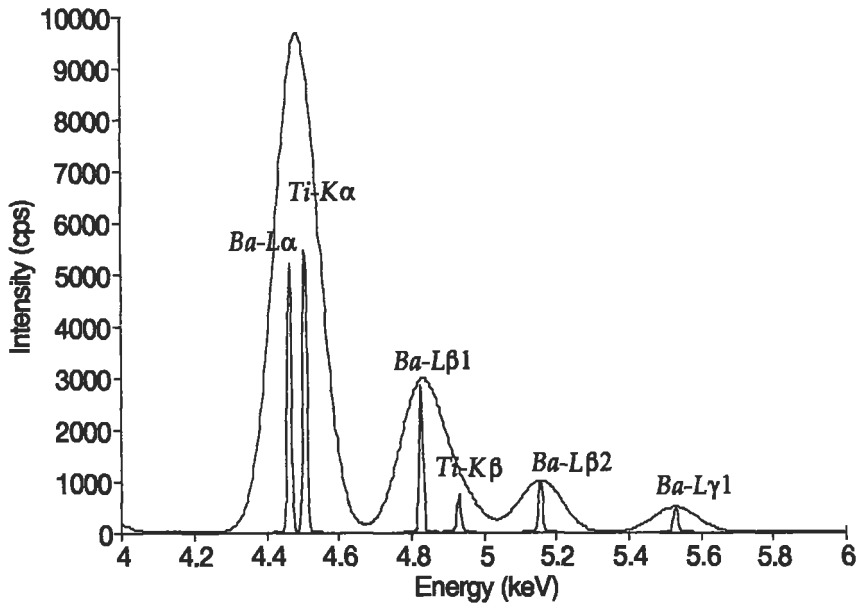
Figure 4 Superposed EDS and WDS spectra from $BaTiO_3$. The EDS spectrum was obtained with a detector having 135-eV resolution, and shows the strongly overlapped Ba $L\alpha_1$–Ti $K\alpha$ and Ba $L\beta_1$–Ti $K\beta$ peaks. The WDS spectrum from the same material shows the peaks to be completely resolved.

The MDL, or trace element sensitivity, is inversely proportional to P^2/B, the ratio of the peak counting rate and the background counting rate for a pure element. If data is collected on both EDS and WDS instruments using the low probe current appropriate to EDS (a few nA) the MDL with EDS will be 3–5× better than that obtained with WDS. But if WDS is used at its normally higher probe currents (20–100 nA) the MDL obtained using WDS will be about 10× better! The major obstacle to a lower MDL in EDS, aside from the peak overlap problem, is a much higher background (due to bremsstrahlung radiation) and therefore a much lower P^2/B ratio relative to WDS. In cases where the peaks are not overlapping it should be possible to detect and analyze 0.1–0.2 nm (about one monolayer) of a metal film on a conducting substrate using EDS.

Sample Requirements

Almost any size solid sample can be studied in the SEM or EPMA. The only limitation is the size of the specimen chamber, which is usually at least 10 cm in diameter. In a standard SEM, however, the *x–y* translation is usually limited to 25 mm. In SEMs with an air lock for sample exchange, the maximum sample size may be only 3–5 cm in diameter. A highly polished surface is required for accurate quanti-

tative analysis, since surface roughness will cause undue absorption of the generated X-ray signal, which is difficult to account for in the quantification procedure. Powder samples can be compacted or fixed in epoxy and analyzed in the SEM or EPMA. However, with the high vacuum required in the electron column, liquids are not easily studied. In the TEM, the sample must be transparent to the incident electrons and therefore may be only a few hundred nm thick. The maximum sample diameter is usually 3 mm. In electron column instruments, nonconducting samples usually present a problem due to excess charge build-up. To provide a conducting path to ground they are coated with a thin conducting film of C or Al, which must be accounted for in the final analysis if the absorption by the coating material is significant. For EDS combined with an X-ray tube generator or radioactive source in air, most of these restrictions are relaxed and almost any sample can be analyzed. Coating is not required for nonconducting specimens. As mentioned before, samples with rough surfaces, such as fracture samples, may give a spectrum, but the relative accuracy of the quantitative analysis will not be very good.

Operational Considerations in Electron Microscopes

For inner shell ionization to take place, the energy of the incident radiation must be greater than the ionization energy of the particular atomic shell in question. For electrons, the ionization cross section σ is calculated using a function of the form $(1/U)\ln U$, where $U = E_0/E_c$ is the ratio of the energy of the incident electron E_0 to the critical ionization energy E_c. Qualitative evaluation of this function shows that σ reaches a maximum around $U = 2.5$, but is almost constant for $U > 2$. To a first approximation, therefore, the only requirement is that the accelerating voltage of the electron gun be chosen such that $U > 2$.

In the analysis of trace elements or thin films on substrate using electrons, however, one finds that the MDL, may be increased by choosing E_0 such that U is just greater than 1. The reason for this is that the k factor, which is the ratio of the intensity from the sample to that from the standard, increases as U approaches 1 for thin films. Thus, by maximizing the k factor, the sensitivity is increased. For bulk sample analysis, however, the k factor will usually be a maximum at $U \sim 2.5$.

Another consideration in the determination of the optimum E_0 is the depth of X-ray production in bulk samples, especially if one component strongly absorbs the radiation emitted by another. This is often the case when there is a low-Z element in a high-Z matrix, e.g., C in Fe. Here X rays from carbon generated deep within the sample will be highly absorbed by the Fe and will not exit the sample to be detected. The usual result will be an erroneously low value for the carbon concentration. In these situations the best choice for E_0 will be closer to E_c with $U \approx 1$ rather than a much higher value with $U = 2.5$.

X-ray line E_c (keV)	C Ka 0.283	Si Ka 1.838	Cr Ka 5.988	Cu Ka 8.980	Au La 11.919	K–O Electron range
Matrix element	Range (μm) for E_0 = 20 keV					
Si	4.737	4.653	4.108	3.496	2.743	4.741
Cr	1.760	1.729	1.526	1.299	1.019	1.761
Ag	1.376	1.351	1.193	1.015	0.797	1.377
Au	0.861	0.846	0.747	0.636	0.499	0.862
	Range (μm) for E_0 = 10 keV					
Si	1.486	1.402	0.857	0.245	*	1.490
Cr	0.552	0.521	0.318	0.091	*	0.554
Ag	0.432	0.407	0.249	0.071	*	0.433
Au	0.27	0.255	0.156	0.045	*	0.271

* = no X rays generated.

Table 1   Range of X-ray generation calculated by the Kanaya-Okayama (K–O) equation for selected X-ray lines in low- to high-density materials for two incident electron energies, E_0. For comparison, the range of electrons with E_c = 0, is given in the last column. (Here E_0 is the incident electron energy, E_c is the critical ionization energy, A is the atomic weight, Z is the atomic number, and ρ is the density.) The K–O X-ray range is given by the equation: R= 0.0276 $A(E_0^{1.67} - E_c^{1.67})$ / $(Z^{0.889}\rho)$ μm.

Range and Lateral Resolution of X-Ray Generation

The range over which characteristic X rays are generated depends both on the properties of the sample and the choice of accelerating voltage. X-ray generation ranges calculated for low-, medium- and high-density materials under a few electron-accelerating voltages are given in Table 1 to illustrate this point. For comparison, the electron range is included in the table. As can be seen, the X-ray generation range is always less than the electron range because characteristic X rays are generated only when the electron has energy greater than E_c. But as can be seen in the table, the difference between the X-ray range and the electron range is very significant only when E_c is nearly equal to E_0. Accordingly, the X-ray generation volume is smaller than the electron interaction volume and the volume from which the X rays are measured is even smaller because of X-ray absorption. (Another discussion of this topic can be found in the article on EPMA.)

It also should be recognized that the density of X-ray production is not constant throughout the X-ray generation volume, but is related to the number and length of electron trajectories per unit volume and the average overvoltage along each trajectory. The distribution of the generated X rays as a function of the mass thickness, or depth, in the sample is given by a mathematical expression that has the shape of a Gaussian curve offset at the surface of the sample. This function is often called the $\phi(\rho z)$ function.

The lateral resolution of X-ray analysis in an SEM or EPMA is not generally related to the incident probe size. From the values for the X-ray generation ranges given in Table 1 one can see that the diameter of the X-ray generation volume in thick samples is much greater than a few tens of nm, which would be the nominal diameter of a medium-resolution probe in an SEM. On the other hand, with a thin-foil sample in a TEM, the probe size will be very important in the determining the lateral resolution, since most of the incident electrons pass through the foil with only a few collisions and therefore are not be deflected far from their incident direction.

Modes of Analysis

There are three modes of analysis commonly used: spectrum acquisition; spatial distribution, or dot, mapping of the elements; and elemental line scans.

In the spectrum acquisition mode the probe is either fixed in the spot mode or raster scanned over a small area at high magnification and a complete spectrum acquired. A typical spectrum is shown in Figure 2.

In an electron microscope or microprobe with scanning capability, data from more than 15 elements can be collected simultaneously and used to generate X-ray dot maps displaying the spatial distribution of the elements in the sample. In this technique the brightness of the CRT is modulated as the beam is raster scanned to reflect the X-ray output of the element of interest, which usually is designated by defining a region of interest (ROI) around the peaks in the EDS spectrum at that point. Some analyzers provide the capability to remove the background from the signal before plotting. Multielement maps can be made with a color CRT, using a different color chosen for each element. These maps can be arranged in an overlay with the colors combined to show the presence of various compounds. A long data collection time, sometimes hours, is often required to collect enough data points for a high-resolution dot map.

With the same scanning capability, it is much faster and often more useful to simply scan one line on a sample. The data is again output to a color CRT, but it is presented as the modulation of the y-amplitude, which is determined by the intensity of the X-ray signal production from the ROI of the element of interest. As the probe scans along the line, the CRT plots a graph of the elemental counting rates versus distance. Here again, it is usually possible to plot the data from many ele-

ments simultaneously. This mode of display will usually show minor concentration differences much better than the brightness modulation technique used in mapping.

Quantification

The ultimate goal in using an EDS analytical system is to be able to measure the concentrations of all the elements in the sample. To this end, a series of measurements are made in which the peak intensity from each element in the sample is compared to the peak intensity obtained from a reference standard using the same operating conditions. The ratio of these two intensities is the k factor mentioned previously. To convert the measured k factors to the composition, it is usually necessary to make corrections that account for deviations from a linear relationship between the k factor and the composition. These include an atomic number correction accounting for the fraction of electrons backscattered by the sample and the volume of X-ray generation (the Z factor); a correction for the absorption of the generated X rays in the sample (the A factor); and a correction for secondary X-ray fluorescence in the sample (the F factor). Various procedures have been developed to do this; the most common is known as the ZAF correction, with $C(\%) = kZAF$.

In another approach, which was previously mentioned, the mass thickness, or depth distribution of characteristic X-ray generation and the subsequent absorption are calculated using models developed from experimental data into a $\phi(\rho z)$ function. Secondary fluorescence is corrected using the same F factors as in ZAF. The $\phi(\rho z)$ formulation is very flexible and allows for multiple boundary conditions to be included easily. It has been used successfully in the study of thin films on substrates and for multilayer thin films.

Conclusions

EDS is an extremely powerful analytical technique of special value in conjunction with electron column instruments. In a few seconds a qualitative survey of the elements present in almost any sample can be made, and in only a few minutes sufficient data can be collected for quantification. The most frequent application has been to highly polished metal samples, although nonconducting samples may be studied if they can be coated with a thin conducting film. Sample dimensions are usually not a problem in an SEM. Most of the detectors used to date have been of the Si (Li) type, but with improvements in the processing methods of germanium, HPGe detectors may start impacting the market. New cooling methods, e.g., Peltier cooling, are being studied and will be a significant improvement if the ultimate temperature can be lowered to nearer to liquid nitrogen temperatures. Detector resolution is still the most serious problem. It is slowly being reduced through improvements in FET design and new methods of charge restoration. New window

materials have made low-Z detectors the standard, opening up the prospects of light element analysis. However, the sensitivity for light elements is generally low and the analytical methods are still being developed because the peak shapes are often not Gaussian and the mass absorption coefficients for the low-Z elements are not very well known.

Overall a "customer" needs to know under what circumstances it is best to use either the electron-beam techniques of EDS and WDS or the X-ray technique of XRF for an analysis problem. If both are equally available, the choice usually resides in whether high spatial resolution is needed, as would be obtained only with electron-beam techniques. If liquids are to be analyzed, the only viable choice is XRF. If one's choice is to use electron-beam methods, the further decision between EDS and WDS is usually one of operator preference. That is, to commence study on a totally new sample most electron-beam operators will run an EDS spectrum first. If there are no serious peak overlap problems, then EDS may be sufficient. If there is peak overlap or if maximum sensitivity is desired, then WDS is usually preferred. Factored into all of this must be the beam sensitivity of the sample, since for WDS analysis the beam current required is 10–100× greater than for EDS. This is of special concern in the analysis of polymer materials.

Related Articles in the Encyclopedia

EPMA, STEM, TEM, SEM, XRF

Bibliography

1   R. Woldseth. *X-Ray Energy Spectrometry.* Kevex Corporation, San Carlos, 1973. A good introduction with emphasis on detectors and electronics. Most of the applications refer to X-ray tube sources. Unfortunately the book is out of print, but many industrial laboratories may have copies.

2   *Quantitative Electron-Probe Microanalysis.* (V. D. Scott and G. Love, eds.) John Wiley & Sons, New York, 1983. Taken from a short course on the electron microprobe for scientists working in the field. A thorough discussion of EDS and WDS is given, including experimental conditions and specimen requirements. The ZAF correction factors are treated extensively, and statistics, computer programs and Monte Carlo methods are explained in detail. Generally, a very useful book.

3   J. I. Goldstein, D. E. Newbury, P. Echlin, D. C. Joy, C. Fiori, and E. Lifshin. *Scanning Electron Microscopy and X-Ray Analysis.* Plenum Press, New York, 1981. Developed from a short course held annually at Lehigh University. The book is concerned with the use and applications of SEM. In the latter context a lengthy discussion of EDS is given. The discussion

on analysis is not as thorough as that in Scott and Love, but serves as an excellent introduction, with all the important topics discussed.

4 D. B. Williams. *Practical Analytical Electron Microscopy in Materials Science.* Verlag Chemie International, Weinheim, 1984. A good monograph discussing the use and applications of AEM, especially at intermediate voltages. The discussion on EDS is an excellent primer for using X-ray analysis on a TEM.

5 *Principles of Analytical Electron Microscopy.* (D. C. Joy, A. D. Romig, and J. I. Goldstein, eds.) Plenum Press, New York, 1986. Another book, more readily available, discussing all aspects of AEM. Approximately one-quarter of the book is devoted to EDS and a discussion of thin-film analysis in the TEM.

3.2 EELS

Electron Energy-Loss Spectroscopy in the Transmission Electron Microscope

NESTOR J. ZALUZEC

Contents

- Introduction
- Basic Principles
- Low-Loss Spectroscopy
- Inner Shell Spectroscopy
- Quantification
- Limitations and Specimen Requirements
- Conclusions

Introduction

Electron Energy-Loss Spectroscopy (EELS) is an analytical methodology which derives its information from the measurement of changes in the energy and angular distribution of an initially nominally monoenergetic beam of electrons that has been scattered during transmission through a thin specimen. This geometry is identical to that which is used routinely in a transmission or Scanning Transmission Electron Microscope (TEM or STEM), and thus in the last decade the technique has been closely associated with these two types of instruments. EELS is an absorption spectroscopy and is similar in many respects to X-Ray Absorption Spectroscopy (XAS). Its characteristic spectral signature, termed the edge profile, is derived from the excitation of discrete inner shell levels to empty states above the Fermi level. Conservation of energy requires that the incident electron beam lose the corresponding amount of energy and intensity expended in exciting each inner shell level, and these are the parameters which are recorded in each experiment. From an analysis of the transmitted electron intensity distribution, the experiment can

derive the local elemental concentration of each atomic species present. Additionally, by studying the detailed shape of the spectral profiles measured in EELS, the analyst may derive information about the electronic structure, chemical bonding, and average nearest neighbor distances for each atomic species detected. A related variation of EELS is Reflection Electron Energy-Loss Spectroscopy (REELS). In REELS the energy distribution of electrons scattered from the surface of a specimen is studied. Generally REELS deals with low-energy electrons (< 10 keV), while TEM/STEM-based EELS deals with incident electrons having energies of 100–400 keV. In this article we shall consider only the transmission case. REELS is discussed in Chapter 5.

In principle, EELS can be used to study all the elements in the periodic table; however, the study of hydrogen and helium is successful only in special cases where their signals are not masked by other features in the spectrum. As a matter of experimental practicality, the inner shell excitations studied are those having binding energies less than about 3 keV. Quantitative concentration determinations can be obtained for the elements $3 \leq Z \leq 35$ using a standardless data analysis procedure. In this range of elements, the accuracy varies but can be expected to be ±10–20% at. By using standards the accuracy can be improved to ±1–2% at. Detection limit capabilities have improved over the last decade from $\sim 10^{-18}$ g to $\sim 10^{-21}$ g. These advances have arisen through improved instrumentation and a more complete understanding of the specimen requirements and limitations. The energy resolution of the technique is limited today by the inherent energy spread of the electron source used in the microscope. Conventional thermionic guns typically exhibit an energy spread of 2–3 eV, and LaB_6 a spread of about 1–2 eV; field emission sources operate routinely in the 0.25–1 eV range. In all cases, the sample examined must be extremely thin (typically < 2000 Å) to minimize the adverse effects of multiple inelastic scattering, which can, in the worse cases, obscure all characteristic information.

The uniqueness and desirability of EELS is realized when it is combined with the power of a TEM or STEM to form an Analytical Electron Microscope (AEM). This combination allows the analyst to perform spatially resolved nondestructive analysis with high-resolution imaging (< 3 Å). Thus, not only can the analyst observe the microstructure of interest (see the TEM article) but, by virtue of the focusing ability of the incident beam in the electron microscope, he or she can simultaneously analyze a specific region of interest. Lateral spatial resolutions of regions as small as 10 Å in diameter are achievable with appropriate specimens and probe-forming optics in the electron microscope.

Basic Principles

EELS is a direct result of the Coulombic interaction of a fast nearly monochromatic electron beam with atoms in a solid. As the incident probe propagates through the
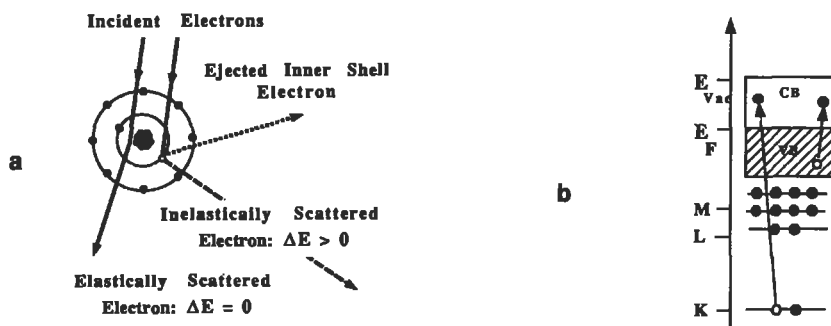
Figure 1 (a) Excitation of inner shells by Coulombic interactions. (b) Energy level diagram illustrating excitation from inner shell and valence band into the conduction band and the creation of a corresponding vacancy.

specimen it experience elastic scattering with the atomic nuclei and inelastic scattering with the outer electron shells (Figure 1a). The inelastic scattering, either with the tightly bound inner shells or with the more loosely bound valence electrons, causes atomic electrons to be excited to higher energy states or, in some cases, to be ejected completely from the solid. This leaves behind a vacancy in the corresponding atomic level (Figure 1b). The complementary analysis techniques of X-ray and Auger spectroscopy (covered in other articles in this book) derive their signals from electron repopulation of the vacancies created by the initial excitation event. After the interaction, the energy distribution of the incident electrons is changed to reflect this energy transfer, the nature and manifestation of which depends upon the specific processes that have occurred. Because EELS is the primary interaction event, all the other analytical signals derived from electron excitation are the result of secondary decay processes. EELS, therefore, yields the highest amount of information per inelastic scattering event of all the electron column-based spectroscopies.

Historically, EELS is one of the oldest spectroscopic techniques based ancillary to the transmission electron microscope. In the early 1940s the principle of atomic level excitation for light element detection capability was demonstrated by using EELS to measure C, N, and O. Unfortunately, at that time the instruments were limited by detection capabilities (film) and extremely poor vacuum levels, which caused severe contamination of the specimens. Twenty-five years later the experimental technique was revived with the advent of modern instrumentation.[1] The basis for quantification and its development as an analytical tool followed in the mid 1970s. Recent reviews can be found in the works by Joy, Maher and Silcox;[2] Colliex;[3] and the excellent books by Raether[4] and Egerton.[5]
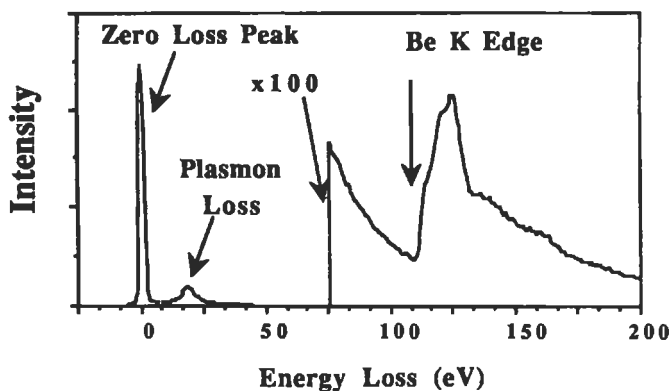
Figure 2   Example of an energy-loss spectrum, illustrating zero loss, and low-loss valence band excitations and the inner shell edge. The onset at 111 eV identifies the material as beryllium. A scale change of 100× was introduced at 75 eV for display purposes.

Figure 2 is an experimental energy-loss spectrum measured from a thin specimen of beryllium. At the left, at zero energy loss, is a large, nearly symmetric peak which represents electrons that have passed through the specimen suffering either negligible or no energy losses. These are the elastically scattered and phonon-scattered incident electrons. Following this peak is the distribution of inelastically scattered electrons, which is generally broken up into two energy regimes for simplicity of discussion. The low-loss regime extends (by convention) from about 1 eV to 50 eV, and exhibits a series of broad spectral features related to inelastic scattering with the valence electron structure of the material. In metallic systems these peaks arise due to a collective excitation of the valence electrons, and are termed *plasmon* oscillations or peaks. For most materials these peaks lie in energy range 5–35 eV.

Beyond this energy and extending for thousands of eV one observes a continuously decreasing background superimposed upon which are a series of "edges" resulting from electrons that have lost energy corresponding to the creation of vacancies in the deeper core levels of the atom (K, $L_3 L_2$, L_1, M_5, and so forth). The edges are generally referred to by the same nomenclature as used in X-ray absorption spectroscopy. The energy needed to ejected electrons amounts to the binding energy of the respective shell (Figure 1b), which is characteristic for each element. By measuring the threshold energy of each edge the analyst can determine the identity of the atom giving rise to the signal, while the net integrated intensity for the edge can be analyzed to obtain the number of atoms producing the signal. This is the basis of quantitative compositional analysis in EELS.
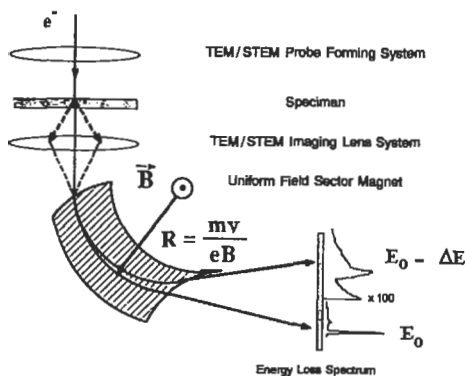
Figure 3   **Schematic representation of EELS analyzer mounted on a TEM / STEM.**

The energy regime most frequently studied by EELS is 0–3 keV. Higher energy losses can be measured; however, a combination of instrumental and specimen-related limitations usually means that these higher loss measurements are more favorable for study by alternative analytical methods, such as X-ray energy-dispersive spectroscopy (see the article on EDS). The practical consequence of this upper energy limit is that for low-Z elements ($1 \leq Z \leq 11$) one studies K-shell excitation; for medium-Z materials ($12 \leq Z \leq 45$), L shells; and for high-Z solids ($19 \leq Z \leq 79$), M, N, and O shells (the latter for $Z > 46$). It is also important to realize that not all possible atomic levels are observed in EELS as edges. The transitions from initial states to final states generally must obey the quantum number selection rules: $\Delta j = 0, \pm 1$, and $\Delta l = \pm 1$. Hence some atomic energy levels, although discrete and well defined, are not discernible by EELS.

Hydrogen and helium are special cases that should be mentioned separately. These elements have absorption edges at ~13 eV and 22 eV, respectively. These values lie in the middle of the low-loss regime, which is dominated by the valence band scattering. Thus, while the physics of inelastic scattering processes dictates that the edges will be present, usually they will be buried in the background of the more intense valence signal. In special cases, for example, when the plasmon losses are well removed, or when the formation of hydrides[6] occurs, presence of hydrogen and helium may be measured by EELS.

The instrumentation used in EELS is generally straightforward. Most commercial apparatus amount to a uniform field magnetic sector spectrometer located at the end of the electron-optical column of the TEM or STEM (Figure 3). Electrons that have traversed the specimen are focused onto the entrance plane of the spectrometer using the microscope lenses. Here the electrons enter a region having a uniform magnetic field aligned perpendicular to their velocity vector, which causes them to be deflected into circular trajectories whose radii vary in proportion to their

velocity or energy and inversely with the magnetic field strength ($R = [m_0 v] / eB$). Location of a suitable detector system at the image plane of the spectrometer then allows the analyst to quantitatively measure the velocity–energy distribution. More complex spectrometers that use purely electrostatic or combined electrostatic and electromagnetic systems have been developed; however, these have been noncommercial research instruments and are not used generally for routine studies. More recently, elaborate imaging spectrometers also have been designed by commercial firms and are becoming incorporated into the column of TEM instruments. These newer instruments show promise in future applications, particularly in the case of energy-loss filtered imaging.

Low-Loss Spectroscopy

As we outlined earlier, the low-loss region of the energy-loss spectrum is dominated by the collective excitations of valence band electrons whose energy states lie a few tens of eV below the Fermi level. This area of the spectrum primarily provides information about the dielectric properties of the solid or measurements of valence electron densities. As a fast electron loses energy in transmission through the specimen its interaction—i.e., the intensity of the measured loss spectrum $I(E)$—can be related to the energy-loss probability $P(E, q)$, which in turn can be expressed in terms of the energy-loss function $Im[-\varepsilon^{-1}(E, q)]$ from dielectric theory.[4] Here q is the momentum vector, and $\varepsilon = (\varepsilon_1 + i \varepsilon_2)$ is the complex dielectric function of the solid.[4] By applying a Kramers–Kronig analysis to the energy-loss function ($Im [-\varepsilon^{-1}(E, q)]$), the real and imaginary parts (ε_1, ε_2) of the dielectric function can be determined. Using ε_1 and ε_2, one can calculate the optical constants (the refractive index η, the absorption index κ, and the reflectivity R) for the material being examined.[3-5]

In addition to dielectric property determinations, one also can measure valence electron densities from the low-loss spectrum. Using the simple free electron model one can show that the bulk plasmon energy (E_p) is governed by the equation:

$$E_p = \frac{h\omega_p}{2\pi} = \sqrt{\eta \frac{h^2 e^2}{4\pi^2 m \varepsilon_0}} \tag{1}$$

where e is the electron charge, m is its mass, ε_0 is the vacuum dielectric constant, h is Planck's constant, and η is the valence electron density. From this equation we see that as the valence electron density changes so does the energy of the plasmon-loss peak. Although this can be applied to characterization, it is infrequently done today, as the variation in E_p with composition is small[7] and calibration experiments must be performed using composition standards. A recent application is the use of plasmon losses to characterize hydrides in solids.[6] Figure 4 shows partial EELS spectra from Mg, Ti, Zr, and their hydrides. The shift in the plasmon-loss peaks
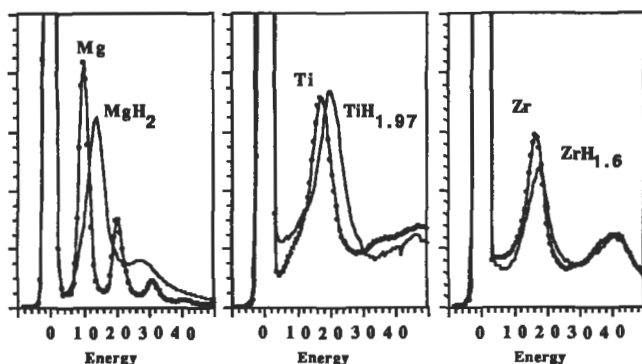
Figure 4   Experimental low-loss profiles for Mg (10.0), Ti (17.2), Zr(16.6), and their hydrides MgH_2 (14.2), $TiH_{1.97}$ (20.0), and $ZrH_{1.6}$ (18.1). The values in parentheses represent the experimental plasmon-loss peak energies in eV.

shows that the addition of hydrogen acts to increase the net electron density in these materials.

Inner Shell Spectroscopy

The most prominent spectral feature in EELS is the inner shell edge profile (Figure 2). Unlike EDS, where the characteristic signal profiles are nominally Gaussian-shaped peaks, in EELS the shape varies with the edge type (K, L, M, etc.), the electronic structure, and the chemical bonding. This is illustrated in Figure 5, which compares spectra obtain from a thin specimen of NiO using both windowless EDS and EELS. The difference in spectral profiles are derived from the fact that different mechanisms give rise to the two signals.

In the case of X-ray emission, the energy of the emitted photon corresponds to the energy differences between the initial and final states when a higher energy level electron repopulates the inner shell level, filling the vacancy created by the incident probe (Figure 1b). These levels are well defined and discrete, corresponding to deep core losses. The information derived is therefore mainly representative of the atomic elements present, rather than of the nuances of the chemical bonding or electronic structure. EDS is most frequently used in quantitative compositional measurements, and its poor energy resolution ~100 eV is due to the solid state detectors used to measure the photons and not the intrinsic width of the X-ray lines (about a few eV).

By contrast, in EELS the characteristic edge shapes are derived from the excitation of discrete inner shell levels into states above the Fermi level (Figure 1b) and reflect the empty density of states above E_F for each atomic species. The overall
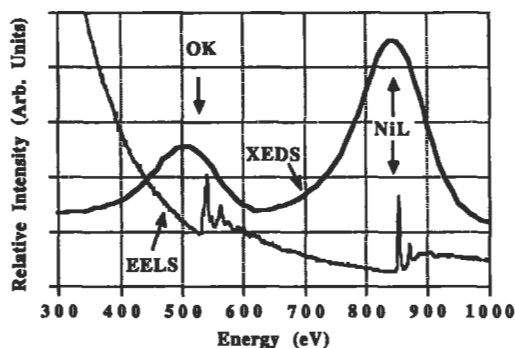
Figure 5   Comparison of spectral profiles measured from a specimen of NiO using EDS and EELS. Shown are the oxygen K- and nickel L-shell signals. Note the difference in the spectral shape and peak positions, as well as the energy resolution of the two spectroscopies.

shape of an edge can be approximately described using atomic models, due to the fact that the basic wavefunctions of deep core electrons do not change significantly when atoms condense to form a solid. Thus, the different edge profiles can be sketched as shown in Figure 6. K-shell edges (s → p transitions) tend to have a simple hydrogenic-like shape. L-shell edges (p → s and p → d transitions) vary between somewhat rounded profiles ($11 \leq Z \leq 17$) to nearly hydrogenic-like, with intense "white lines" at the edge onset ($19 \leq Z \leq 28$, and again for $38 \leq Z \leq 46$). In the fourth and fifth periods, these white lines are due to transitions from p to d states. M shells generally tend to be of the delayed-onset variety, due to the existence of an effective centrifugal barrier that is typical of elements with final states having large l quantum numbers. White lines near the M-shell edge onsets are observed when empty d states ($38 \leq Z \leq 46$) or f states ($55 \leq Z \leq 70$) occur, as in the case of the L shells. N and O shells are variable in shape and tend to appear as large, somewhat symmetrically shaped peaks rather than as "edges."

Figure 6   Schematic illustration of K, L, M, N and O edge shapes; the "white lines" sometimes detected on L and M shells are shown as shaded peaks at the edge onsets. In all sketches the background shape has been omitted for clarity.
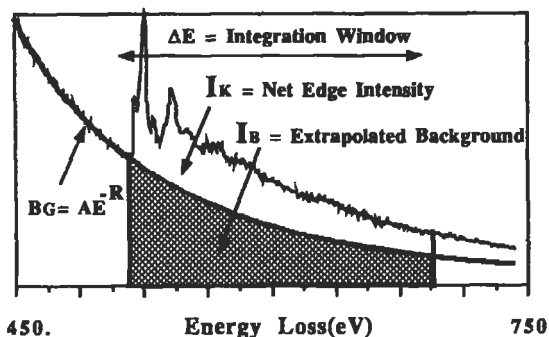
Figure 7   Details of oxygen K shell in NiO, illustrating NES and EXELFS oscillations and the measurement of the integrated edge intensity I_K used for quantitative concentration determination.

It is important to note that although specific edge profiles follow these generic shapes somewhat, they can deviate significantly in finer details in the vicinity of edge onsets. This structure arises due to solid state effects, the details of which depend upon the specific state (both electronic and chemical) of the material under scrutiny. Because of this strong variation in edge shape, experimental libraries of edge profiles also have been documented[8, 9] and have proven to be extremely useful supplementary tools. (Calculation of the detailed edge shape requires a significant computational effort and is not currently practical for on-line work.) These solid state effects also give rise to additional applications of EELS in materials research, namely: measurements of the d-band density of states in the transition metal systems,[10] and chemical state determinations[11] using the near-edge structure. The former has been used successfully by several research groups, while the latter application is, as yet, seldom used today in materials science investigations.

A more detailed description of near edge structure requires that one abandon simple atomic models. Instead, one must consider the spectrum to be a measure of the *empty local density of states above the Fermi level* of the elemental species being studied, scaled by the probability that the particular transition will occur. A discussion of such an undertaking is beyond the scope of this article, but EELS derives its capabilities for electronic and chemical bonding determinations from the near-edge structure. Calculation of this structure, which is due to the joint density of states, is involved and the studies of Grunes et al.[12] represent some of the most complete work done to date. The near-edge structure covers only the first few tens of eV beyond the edge onset; however, as we can see intensity oscillations extend for hundreds of eV past the edge threshold. This extended energy-loss fine structure (EXELFS) is analogous to the extended absorption fine structure (EXAFS) visible in X-ray absorption spectroscopy. An example of these undulations can be seen in the weaker oscillations extending beyond the oxygen K edge of Figure 7. The anal-

ysis of EXELFS oscillations can be taken virtually from the EXAFS literature and applied to EELS data, and allows the experimentalist to determine the nearest neighbor distances and coordination numbers about individual atomic species.[13]

Quantitative Concentration Measurements

The principles of quantitative concentration measurement in EELS is straightforward and simpler than in EDS. This is due to the fact that EELS is the primary interaction event, while all other electron-column analytical techniques are the result of secondary decay or emission processes. Thus, all other electron microscope-based analytical spectroscopies (EDS, Auger, etc.) must incorporate into their quantitative analysis procedures, corrections terms to account for the variety of competing processes (atomic number effects, X-ray fluorescence yields, radiative partition functions, absorption, etc.) that determine the measured signal. In EELS, the net integrated intensity in the kth edge profile for an element corresponds simply to the number of electrons which have lost energy due to the excitation of that particular shell. This is related to the incident electron intensity (I_0) multiplied by the cross section for ionization of the kth edges σ_K times the number of atoms in the analyzed volume (N):

$$I_K = N\sigma_K I_0 \qquad (2)$$

Here I_K is the net intensity above background over an integration window of ΔE (Figure 7), while I_0 is the integrated intensity of the zero-loss peak (Figure 2). Generally the background beneath an edge is measured before the edge onset and extrapolated underneath the edge using a simple relationship for the background shape: $BG = AE^{-R}$. Here E is the energy loss, and A and R are fitting parameters determined experimentally from the pre-edge background. From Equation (2), one can express the absolute number of atoms/cm^2 as:

$$N = \frac{I_K}{\sigma_K I_0} \qquad (3)$$

Hence by measuring I_K and I_0 and assuming σ_K is known or calculable, the analyst can determine N. Using a hydrogenic model, Egerton[5] has developed a set of FORTRAN subroutines (SigmaK and SigmaL) that are used by the vast majority of analysts for the calculation of K- and L-shell cross sections for the elements lithium through germanium. Leapman et al.[14] have extended the cross section calculations. Using an atomic Hartree-Slater program they have calculated K-, L-, M-, and some N-shell cross sections, however, these calculations are not amenable to use on an entry-level computer and require substantial computational effort.[14] They do, however, extend the method beyond the limits of Egerton's hydrogenic model. Tabular compilations of the cross section are generally not available, nor do they

tend to be useful, as parameters used in calculations seldom match the wide range of experimental conditions employed during TEM- or STEM-based analysis.

An alternative approach to the quantitative analysis formalism is the ratio method. Here we consider the ratio of the intensities of any two edges A and B. Using Equation (3) we can show that

$$\frac{N_A}{N_B} = \frac{\sigma_B I_A}{\sigma_A I_B} \tag{4}$$

The elegance of this relationship rests in the fact that all the information one needs to measure the relative concentration ratio of any two elements is simply the ratio of their integrated edge profiles, I_0 having canceled out of the relationship.

This ratio method is generally the most widely used technique for quantitative concentration measurements in EELS. Unfortunately, the assumptions used in deriving this simple relationship are never fully realized. These assumptions are simply that electrons scattering from the specimen are measured over *all* angles and for *all* energy losses. This is physically impossible, since finite angular and energy windows are established or measured in the spectrum. For example, referring to Figure 7, we see that in NiO the Ni L-shell edge is superimposed upon the tail of the oxygen K-shell edge and clearly restricts the integration energy window for oxygen to about 300 eV. Similarly it is impossible in a TEM or STEM to collect all scattered electrons over π sR; an upper limit of about 100 mR is practically attainable. A solution to this problem was devised by Egerton[5] and can be incorporated into Equations (3) and (4) by replacing I_A by $I_A(\Delta E, \beta)$ and σ_A by $\sigma_A(\Delta E, \beta)$, since we measure over a finite energy (ΔE) and angular window (β). The quantity $\sigma_A(\Delta E, \beta)$ is now the partial ionization cross section for the energy and angular windows of ΔE and β, respectively. Using this ratio approach to quantification, accuracies of ± 5–10% at. for the same type edges (i.e., both K or L) have been achieved routinely using Egerton's hydrogenic models. When dissimilar edges are analyzed (for example one K and one L shell), the errors increase to ± 15–20% at. The major errors here result from the use of the hydrogenic model to approximate all edge shapes.

Although these errors may sound relatively large in terms of accuracy for quantification, it is the simplicity of the hydrogenic model that ultimately gives rise to the problem, and not the principle of EELS quantification. Should it be necessary to achieve greater accuracy, concentration standards can be developed and measured to improve accuracy. In this case, standards are used to accurately determine the experimental ratio $(\sigma_B(\Delta E, \beta)/\sigma_A(\Delta E, \beta)$ by measuring I_A/I_B and knowing the composition N_A/N_B. These σ_B/σ_A values are used when analyzing the unknown specimen, and accuracies to ~1% at. can be obtained in ideal cases. When employing standards, it is essential that the near-edge structure does not vary significantly between the unknown and the standard, since in many cases near-edge structure
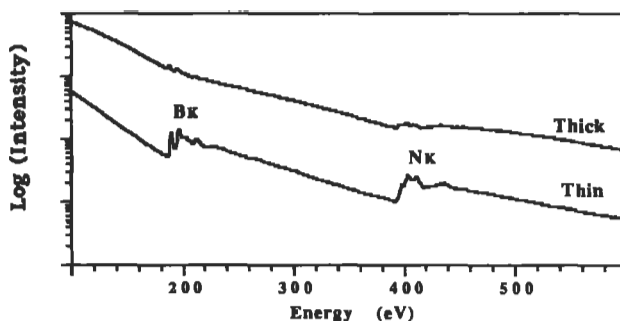
Figure 8 Illustration of the decrease in the edge / background ratio for the B_K (~188 eV) and N_K (~399 eV) shells in EELS. In the data sets, the upper profile is from the thicker region (~2000 Å) of the BN specimen while the lower is thinner (~200 Å). Note the logarithmic vertical scale.

contributes substantially to the net integrated edge profiles. This, unfortunately, is usually a difficult situation to realize. As a practical note, standards often are not used due to the fact that they require the analyst to prepare accurate multielement standards in TEM form for each elemental system to be studied and for every set of operating conditions used during the analysis of the unknown.

Limitations and Specimen Requirements

The single most important limitation to the successful application of EELS to problems in materials characterization relates to the specimen, namely, its thickness. Being a transmission technique it is essential that the incident beam penetrate the specimen, interact, and then enter the spectrometer for detection. As the specimen thickness increases, the likelihood of inelastic scattering increases, and hence the EELS signal increases. Unfortunately, the background signal increases at a faster rate than that of the characteristic edges. This results in the edges becoming effectively lost in the background, as illustrated in Figure 8, which shows the decrease in the edge-to-background ratio obtained from different thicknesses of a specimen of boron nitride. As a general rule, if λ is the mean free path for inelastic scattering, the specimen thickness t should not exceed values of $t/\lambda \approx 1$ and preferably should be < 0.5 to minimize the adverse effects of multiple scattering. The mean free path λ is a function of the atomic number and the accelerating voltage. At 100 kV, λ is about 1200 Å for aluminium, decreasing to ~900 Å at nickel, and reaching ~600 Å for gold. Increasing the accelerating voltage of the electron microscope reduces multiple inelastic scattering somewhat; for example, increasing the incident beam voltage from 100 to 300 kV increases λ by a factor of ~1.8, and going from 100 to 1000 kV yields a factor of ~2.5. However, increasing the voltage introduces another set of problems for the experimentalist, that is, electron irradiation (displacement) damage. In this situation, the high-energy electrons have suffi-

cient energy to displace atoms from their normal lattice sites and, in some cases, literally to sputter holes through the specimen.

Conclusions

The combination of EELS with a TEM or STEM yields a powerful tool for the microcharacterization of materials. Its primary applications are in ultrahigh spatial resolution spectroscopy of thin electron-transparent solids. With optimized specimens, EELS can be used to obtain the local elemental composition of a specific region of interest on the specimen, and with more detailed calculations can provide information concerning the electronic or chemical states of the sample. EELS can be applied to any specimen that can be prepared for observation in the TEM or STEM. Future developments will concentrate in the areas of higher speed data acquisition using one- and two-dimensional parallel detectors for combined spectroscopy and parallel imaging, ultrahigh-energy resolution spectroscopy in the 50–100 meV range, and advanced software to make routine the more complex data analyses.

Related Articles in the Encyclopedia

TEM, STEM, EDS, EXAFS, NEXAFS, XPS, and UPS, REELS

References

1   A. V. Crewe, M. Isaacson, and D. E. Johnson. *Rev. Sci. Instr.* **42,** 411, 1971.

2   *Introduction to Analytical Electron Microscopy.* (J. J. Hren, D. C. Joy, and J. I. Goldstein, eds.) Plenum Press, 1979. A good overview of analytical electron microscopy.

3   C. Colliex. In: *Advances in Optical and Electron Microscopy.* (R. Barer and V.E. Cosslett, eds.) Academic Press, 1984, Volume 9. This chapter contains a concise, but detailed, treatment of EELS with significant references to the major studies done.

4   H. Raether. *Springer Tracts in Modern Physics.* **88,** 1980. This book details the wealth of information contained in the low-loss spectrum, and treats the mathematics in considerable detail.

5   R. F. Egerton. *Electron Energy Loss Spectrometry in the Electron Microscope.* Plenum Press, 1986. This is a comprehensive text on the use of EELS in the TEM. It covers instrumentation, theory and practical applications.

6   N. J. Zaluzec, T. Schober, and B. W. Veal. In: *Analytical Electron Microscopy—1982 Proceedings of the Workshop at Vail Colorado.* San Francisco Press, p. 191.

7   D. B. Williams and J. W. Edington. *J. Microsc.* **108,** 113, 1976.

8   N. J. Zaluzec. *Ultramicroscopy.* **9,** 319, 1982; and *J. de Physique. C2* **45** (2), 1984. This work is also available *gratis* from the author, at EM Center, Argonne National Laboratory Materials Science Division-212, Argonne, IL 60439, USA.

9   C. C. Ahn and O. L. Krivanek. *An Atlas of Electron Energy Loss Spectra.* Available from Gatan Inc., Pleasanton, CA 94566, USA.

10 T. I. Morrison, M. B. Brodsky, and N. J. Zaluzec. *Phys. Rev. B.* **32,** (5) 3107, 1985.

11 M. Isaacson. In: Microbeam Analysis in Biology. (C. P. Lechene and R. R. Warner, eds.) Academic Press, New York, 1979, p.53.

12 L. A. Grunes, R. D. Leapman, C. N. Wilker, R. Hoffmann, and A. B. Kunz. *Phys. Rev. B.* **25,** 7157, 1982.

13 M. M. Disko, O. L. Krivanek, and P. Rez. *Phys. Rev. B.* **25,** 4252, 1982.

14 R. D. Leapman, P. Rez, and D. F. Mayers. *J. Chem. Phys.* **72,** 1232, 1980.

3.3 CL

Cathodoluminescence

B.G. YACOBI

Contents

- Introduction
- Basic Principles
- Instrumentation
- Quantification
- General Applications and Examples
- Artifacts
- Conclusions

Introduction

Cathodoluminescence (CL), i.e., the emission of light as the result of electron-beam bombardment, was first reported in the middle of the nineteenth century in experiments in evacuated glass tubes. The tubes were found to emit light when an electron beam (cathode ray) struck the glass, and subsequently this phenomenon led to the discovery of the electron. Currently, cathodoluminescence is widely used in cathode-ray tube-based (CRT) instruments (e.g., oscilloscopes, television and computer terminals) and in electron microscope fluorescent screens. With the developments of electron microscopy techniques (see the articles on SEM, STEM and TEM) in the last several decades, CL microscopy and spectroscopy have emerged as powerful tools for the microcharacterization of the electronic properties of luminescent materials, attaining spatial resolutions on the order of 1 μm and less.[1] Major applications of CL analysis techniques include:

1 Uniformity characterization of luminescent materials (e.g., mapping of defects and measurement of their densities, and impurity segregation studies)

2   Obtaining information on a material's electronic band structure (related to the fundamental band gap) and analysis of luminescence centers

3   Measurements of the dopant concentration and of the minority carrier diffusion length and lifetime

4   Microcharacterization of semiconductor devices (e.g., degradation of optoelectronic devices)

5   Analysis of stress distributions in epitaxial layers

6   *In-situ* characterization of dislocation motion in semiconductors

7   Depth-resolved studies of defects in ion-implanted samples and of interface states in heterojunctions.

In CL microscopy, luminescence images or maps of regions of interest are displayed, whereas in CL spectroscopy a luminescence spectrum from a selected region of the sample is obtained. The latter is analogous to a point analysis in X-ray microanalysis (see the article on EPMA). However, unlike X-ray emission, cathodoluminescence does not identify the presence of specific atoms. The lines of characteristic X-rays, which are emitted due to electronic transitions between sharp inner-core levels (see the articles on EDS, EPMA, or XRF), are narrow and are largely unaffected by the environment of the atom in the lattice. In contrast, the CL signal is generated by detecting photons (in the ultraviolet, visible, and near-infrared regions of the spectrum) that are emitted as the result of electronic transitions between the conduction band, or levels due to impurities and defects lying in the fundamental band gap, and the valence band. These transition energies and intensities are affected by a variety of defects, by the surface of the material, and by external perturbations, such as temperature, stress, and electric field. Thus, no universal law can be applied in order to interpret and to quantify lines in the CL spectrum. Despite this limitation, the continuing development of CL is motivated by its attractive features:

1   CL is the only contactless method (in an electron probe instrument) that provides microcharacterization of electronic properties of luminescent materials.

2   A CL system attached to a scanning electron microscope (SEM) provides a powerful means for the uniformity studies of luminescent materials with the spatial resolution of less than 1 µm.

3   The detection limit of impurity concentrations can be as low as 10^{14} atoms/cm^3, which is several orders of magnitude better than that of the X-ray microanalysis mode in the SEM.

4   CL is a powerful tool for the characterization of optical properties of wide bandgap materials, such as diamond, for which optical excitation sources are not readily available.

5 Since the excitation depth can be selected by varying the electron-beam energy, depth-resolved information can be obtained.

6 In optoelectronic materials and devices, it is the luminescence properties that are of practical importance.

CL studies are performed on most luminescent materials, including semiconductors, minerals, phosphors, ceramics, and biological–medical materials.

Basic Principles

The Excitation Process

As the result of the interaction between keV electrons and the solid, the incident electron undergoes a successive series of elastic and inelastic scattering events, with the range of the electron penetration being a function of the electron-beam energy: $R_e = (k/\rho) E_b^\alpha$, where E_b is the electron-beam energy, k and α depend on the atomic number of the material and on E_b, and ρ is the density of the material. Thus, one can estimate the so-called generation (or excitation) volume in the material. The generation factor, i.e., the number of electron–hole pairs generated per incident beam electron, is given by $G = E_b (1-\gamma)/E_i$, where E_i is the ionization energy (i.e., the energy required for the formation of an electron–hole pair), and γ represents the fractional electron-beam energy loss due to the backscattered electrons.

Luminescence Processes

The emission of light in luminescence processes is due to an electronic transition (relaxation) between a higher energy state, E_2, and an empty lower energy state, E_1. (The state E_2 is the excited state caused by the electron-beam excitation process.) The energy, or the wavelength of the emitted photon, $h\nu = hc/\lambda = E_2 - E_1$. The wavelength λ (in µm) of a photon is related to the photon energy E (in eV) by $\lambda \cong 1.2398/E$. In wide band-gap materials luminescence occurs in the visible range (from about 0.4 to 0.7 µm, corresponding to about 3.1 to 1.8 eV). In many cases, luminescence also occurs at longer wavelengths in the near-infrared region.

For a simplified case, one can obtain[1] the rate of CL emission, $L_{CL} = f\eta G I_b/e$, where f is a function containing correction parameters of the CL detection system and that takes into account the fact that not all photons generated in the material are emitted due to optical absorption and internal reflection losses;[1] η is the radiative recombination efficiency (or internal quantum efficiency); I_b is the electron-beam current; and e is the electronic charge. This equation indicates that the rate of CL emission is proportional to η, and from the definition of the latter we conclude that in the observed CL intensity one cannot distinguish between radiative and nonradiative processes in a quantitative manner. One should also note that η depends on various factors, such as temperature, the presence of defects, and the
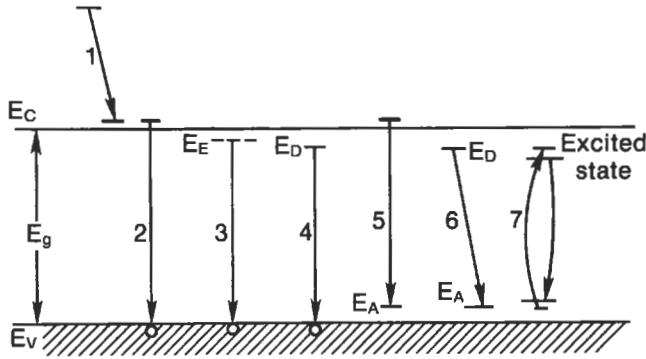
Figure 1   Schematic diagram of luminescence transitions between the conduction band (E_C), the valence band (E_V), and exciton (E_E), donor (E_D,) and acceptor (E_A) levels in the luminescent material.

particular dopants and their concentrations. One result of the analysis of the dependence of the CL intensity on the electron-beam energy indicates the existence at the surface of a dead layer, where radiative recombination is absent.[2]

In inorganic solids, luminescence spectra can be categorized as *intrinsic* or *extrinsic*. Intrinsic luminescence, which appears at elevated temperatures as a near Gaussian-shaped band of energies with its peak at a photon energy $h\nu_p \cong E_g$, is due to recombination of electrons and holes across the fundamental energy gap E_g (see Figure 1). Extrinsic luminescence, on the other hand, depends on the presence of impurities and defects. In the analysis of optical properties of inorganic solids it is also important to distinguish between *direct-gap* materials (e.g., GaAs and ZnS) and *indirect-gap* materials (e.g., Si and GaP). This distinction is based on whether the valence band and conduction band extrema occur at the same value of the wave vector **k** in the energy band $E(\mathbf{k})$ diagram of the particular solid. In the former case, no phonon participation is required during the direct electronic transitions. (A phonon is a quantum of lattice vibrations.) In the latter case, phonon participation is required to conserve momentum during the indirect electronic transitions; since this requires an extra particle, the probability of such a process occurring is significantly lower than that of direct transitions. Thus, fundamental emission in indirect-gap materials is relatively weak compared with that due to impurities or defects.

A simplified schematic diagram of transitions that lead to luminescence in materials containing impurities is shown in Figure 1. In process 1 an electron that has been excited well above the conduction band edge dribbles down, reaching thermal equilibrium with the lattice. This may result in phonon-assisted photon emission or, more likely, the emission of phonons only. Process 2 produces intrinsic luminescence due to direct recombination between an electron in the conduction band

and a hole in the valence band, and this results in the emission of a photon of energy $hv \cong E_g$. Process 3 is the exciton (a bound electron–hole pair) decay observable at low temperatures; free excitons and excitons bound to an impurity may undergo such transitions. In processes 4, 5, and 6, transitions that start or finish on localized states of impurities (e.g., donors and acceptors) in the gap produce extrinsic luminescence, and these account for most of the processes in many luminescent materials. Shallow donor or acceptor levels can be very close to the conduction and valence bands; to distinguish between the intrinsic band-to-band transitions and those associated with shallow impurity transitions, measurements have to be performed at cryogenic temperatures, where CL spectra are sharpened into lines corresponding to transitions between well-defined energy levels. Process 7 represents the excitation and radiative deexcitation of an impurity with incomplete inner shells, such as a rare earth ion or a transition metal. It should be emphasized that lattice defects, such as dislocations, vacancies, and their complexes with impurity atoms, may also introduce localized levels in the band gap, and their presence may lead to the changes in the recombination rates and mechanisms of excess carriers in luminescence processes.

Spatial Resolution

The spatial resolution of the CL-SEM mode depends mainly on the electron-probe size, the size of the excitation volume, which is related to the electron-beam penetration range in the material (see the articles on SEM and EPMA), and the minority carrier diffusion. The spatial resolution also may be affected by the signal-to-noise ratio, mechanical vibrations, and electromagnetic interference. In practice, the spatial resolution is determined basically by the size of the excitation volume, and will be between about 0.1 and 1 μm[1]

Instrumentation

Two general categories of CL analysis systems are wavelength nondispersive-versus-dispersive, and ambient-versus-cryogenic temperature designs. The first category essentially leads to two basic CL analysis methods, microscopy and spectroscopy. In the former case, an electron microscope (SEM or STEM) is equipped with various CL detecting attachments, and thus CL images or maps of regions of interest can be displayed on the CRT. In the latter case an energy-resolved spectrum corresponding to a selected area of the sample can be obtained. CL detector designs differ in the combination of components used[3]. Although most of these are designed as SEM attachments,[3] several CL collection systems were developed in dedicated STEMs.[4] The collection efficiencies of the CL detector systems vary from several percent for photomultipliers equipped with light guides, to close to 90% for systems incorporating ellipsoidal or parabolic mirrors coupled directly to a monochromator. A relatively simple and inexpensive, but powerful, CL detector using an

optical fiber light collection system also has been developed.[5] In these designs, the signal from the photomultiplier can be used to produce micrographs and spectra. When the grating of the monochromator is bypassed, photons of all wavelengths falling on the photomultiplier produce the panchromatic (integral) CL signal. In the dispersive mode, for a constant monochromator setting and a scanning electron-beam condition, monochromatic micrographs can be obtained; and when the monochromator is stepped through the wavelength range of interest and the electron beam is stationary or scans a small area, CL spectra can be derived. The proper choice of a detector is important in CL measurements. In the visible range, photomultipliers are the most efficient detectors. For luminescence in the infrared range, solid state detectors, as well as Fourier transform spectrometry (FTS) can be used. For detailed quantitative analysis, the calibration of the CL detection system for its spectral response characteristics is important in most cases.

Although in many applications noncryogenic CL system designs may be sufficient, for detailed quantitative studies of impurities and defects in various materials it is necessary to use high-efficiency light-collection dispersive systems having the capability of sample cooling, preferably to liquid-helium temperatures. The advantages of sample cooling are to increase the CL intensity, to sharpen the CL spectrum into lines corresponding to transitions between well-defined energy levels that allow the more reliable interpretation of CL spectra, and to reduce the rate of electron bombardment damage in electron-beam sensitive materials.

Another basic approach of CL analysis methods is that of the CL spectroscopy system (having no electron-beam scanning capability), which essentially consists of a high-vacuum chamber with optical ports and a port for an electron gun. Such a system is a relatively simple but powerful tool for the analysis of ion implantation-induced damage, depth distribution of defects, and interfaces in semiconductors.[6]

Optical CL microscopes are instruments that couple electron gun attachments to optical microscopes. Although such systems have a limited spatial resolution, they are used widely in the analysis of minerals.[7]

Quantification

As mentioned above, the interpretation of CL cannot be unified under a simple law, and one of the fundamental difficulties involved in luminescence analysis is the lack of information on the competing nonradiative processes present in the material. In addition, the influence of defects, the surface, and various external perturbations (such as temperature, electric field, and stress) have to be taken into account in quantitative CL analysis. All these make the quantification of CL intensities difficult. Correlations between dopant concentrations and such band-shape parameters as the peak energy and the half-width of the CL emission currently are more reliable as means for the quantitative analysis of the carrier concentration.

a |———| 10 μm   b |—| 10 μm
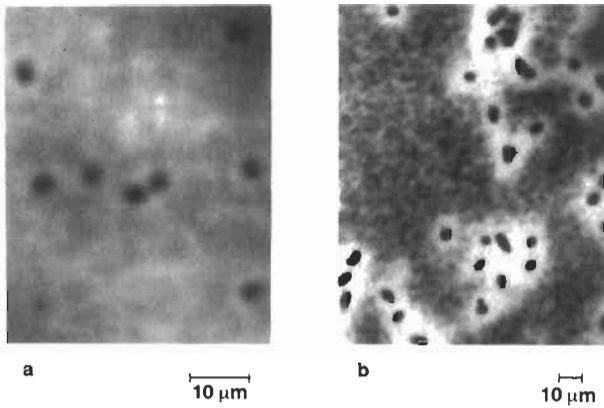
Figure 2   CL micrographs of Te-doped GaAs: dark-dot dislocation contrast (a) in GaAs doped with a Te concentration of 10^{17} cm^{-3}; and dot-and-halo dislocation contrast (b) in GaAs doped with a Te concentration of 10^{18} cm^{-3}.

Nonradiative surface recombination is a loss mechanism of great importance for some materials (e.g., GaAs). This effect, however, can be minimized by increasing the electron-beam energy in order to produce a greater electron penetration range.

A method for quantification of the CL, the so-called MAS corrections, in analogy with the ZAF correction method for X rays (see the article on EPMA), has been proposed[8] to account for the effects of the excess carrier concentration, absorption and surface recombination. In addition, a total internal reflection correction should also be included in the analysis, which leads to the MARS set of corrections. This method can be used for further quantification efforts that also should involve Monte Carlo calculations of the generation of excess carriers.

General Applications and Examples

Major applications of CL microscopy and spectroscopy in the analysis of solids have been listed in the Introduction. Some specific examples of CL applications are outlined below.

An example of the uniformity characterization, as well as of the analysis of the electrically active defects, is shown in Figure 2. These CL micrographs demonstrate two different forms of dislocation contrast (dark-dot and dot-and-halo contrast) for GaAs crystals doped with Te concentrations of 10^{17} cm^{-3} (Figure 2a) and 10^{18} cm^{-3} (Figure 2b). The latter shows variations in the doping concentration around dislocations. This figure also demonstrates that CL microscopy is a valuable tool for determining dislocation distributions and densities in luminescent materi-

├─────┤
2 μm
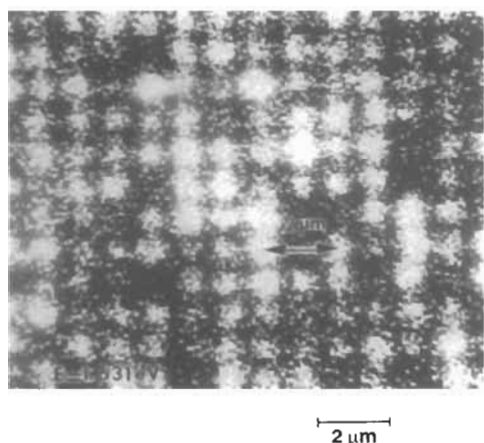
Figure 3   Monochromatic CL image (recorded at 1.631 eV) of quantum well boxes, which appear as bright spots.[9]

als. Reliable measurements of dislocation densities up to about 10^6 cm^{-2} can be made with the CL image.

An example of the CL microcharacterization of an array of GaAs/AlGaAs quantum well (QW) boxes[9] is presented in Figure 3, which shows the CL monochromatic image recorded at the energy corresponding to one of the characteristic luminescence lines (i.e., 1.631 eV). In such structures, the carriers are confined by surrounding a smaller band-gap semiconductor layer with wider band-gap layers. Confinement of carrier motion to 0 degrees of freedom will be obtained for the smaller band-gap layer in the form of a box.[9] The monochromatic CL image shows nonuniformities in the luminescence intensity from one box to another, since not all the QW boxes are identical due to variations in the confining potential between them that result from the presence of residual processing-induced damage.[9]

Cathodoluminescence microscopy and spectroscopy techniques are powerful tools for analyzing the spatial uniformity of stresses in mismatched heterostructures,[10] such as GaAs/Si and GaAs/InP. The stresses in such systems are due to the difference in thermal expansion coefficients between the epitaxial layer and the substrate. The presence of stress in the epitaxial layer leads to the modification of the band structure, and thus affects its electronic properties; it also can cause the migration of dislocations, which may lead to the degradation of optoelectronic devices based on such mismatched heterostructures. This application employs low-temperature (preferably liquid-helium) CL microscopy and spectroscopy in conjunction with the known behavior of the optical transitions in the presence of stress to analyze the spatial uniformity of stress in GaAs epitaxial layers. This analysis can reveal,

a   λ = 818 nm   b   λ = 824 nm   c   λ = 832 nm

|⎯⎯⎯⎯⎯⎯|
100 μm
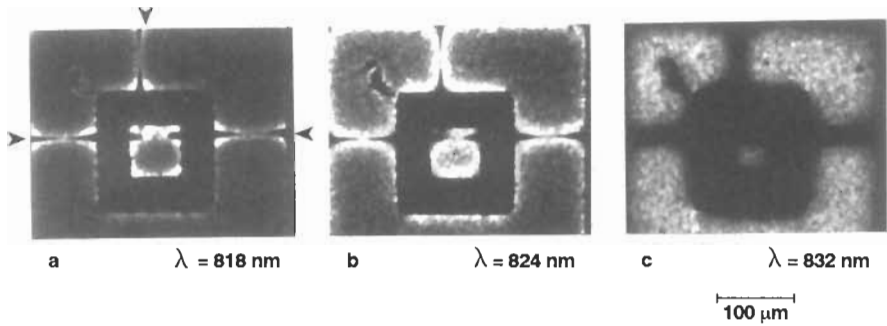
Figure 4   **Monochromatic CL images of the GaAs / Si sample recorded at 818 nm (a), 824 nm (b), and 832 nm (c). Microcracks are indicated by arrows in (a). The sample temperature is about 20 K.**[10]

for example, variations in stress associated with the patterning of GaAs layers grown on mismatched substrates.[10] An example describing stress variations and relief due to patterning in GaAs grown on Si substrates is shown in Figure 4, which presents monochromatic CL images of a GaAs layer at 818, 824, and 832 nm. These images demonstrate that the convex corners and the edges in the patterned regions emit at shorter wavelengths compared to the interiors of these regions. Detailed analysis of the CL spectra in different regions of a GaAs layer indicates strong variations in stress associated with patterning of such layers.[10]

An example of CL depth-resolved analysis of subsurface metal–semiconductor interfaces, using an ultrahigh-vacuum CL system,[6] is shown in Figure 5. This figure presents CL spectra of ultrahigh vacuum-cleaved CdS before and after 50-Å Cu deposition and pulsed laser annealing.[6] The deposition of Cu produces a weak peak at about 1.27 eV, in addition to the CdS band-edge emission at 2.42 eV. Pulsed laser annealing with an energy density of 0.1 J/cm^2 increases the intensity of this peak, which is related to Cu_2S compound formation.[6] This specific example clearly indicates that low-energy CL spectroscopy can be used effectively in the analysis of chemical interactions at buried metal–semiconductor interfaces.

As mentioned earlier, CL is a powerful tool for the characterization of optical properties of wide band-gap materials, such as diamond, for which optical excitation sources are not readily available. In addition, electron-beam excitation of solids may produce much greater carrier generation rates than typical optical excitation. In such cases, CL microscopy and spectroscopy are valuable methods in identifying various impurities, defects, and their complexes, and in providing a powerful means for the analysis of their distribution, with spatial resolution on the order of 1 μm and less.[11]
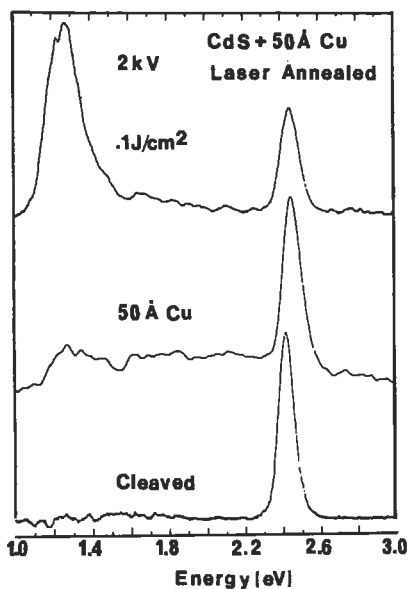
Figure 5 CL spectra of ultrahigh vacuum-cleaved CdS before and after *in situ* deposition of 50 Å of Cu, and after *in situ* laser annealing using an energy density of 0.1 J / cm^2. The electron-beam voltage is 2 kV.[6]

Artifacts

Artifacts in CL analysis of materials may arise from luminescent contaminants, from scintillations caused by backscattered electrons striking components of the CL system, or from incandescence from the electron gun filament reaching the detector. Most of these may be eliminated by chopping the electron beam and detecting the CL signal with a lock-in amplifier. In the CL spectra, ghost peaks may appear due to total internal reflection and self-absorption.[8] Prolonged electron-beam irradiation may cause changes in the CL intensity, localized heating at high beam currents, or may lead to surface contamination of the specimen. To alleviate the latter problem, it is recommended to replace the diffusion pump by a turbomolecular pump, or to use liquid-nitrogen cooled shields around the specimen. Spurious signals also may arise due to charging in nonconducting samples. As a general rule, the electron-beam damage is minimized by maximizing the beam voltage, minimizing the beam current, and using minimum detection times.

It should be noted that during CL observations intensity variations may arise due to sample morphology (e.g., surface roughness), which may lead to nonuniform excitation and to local variations in optical absorption and reflection losses.

Conclusions

In summary, CL can provide contactless and nondestructive analysis of a wide range of electronic properties of a variety of luminescent materials. Spatial resolution of less than 1 μm in the CL-SEM mode and detection limits of impurity concentrations down to 10^{14} at/cm^3 can be attained. CL depth profiling can be performed by varying the range of electron penetration that depends on the electron-beam energy; the excitation depth can be varied from about 10 nm to several μm for electron-beam energies ranging between about 1 keV and 40 keV.

The development of quantitative CL analysis is the most challenging issue. With further development of interpretive theory and with the trend toward the computerization of electron microscopy, quantitative CL analysis should become feasible.

Extensions in wavelength, into both the infrared and the ultraviolet ranges will continue, motivated by increasing interest in narrow band-gap semiconductors and wide band-gap materials.

Applications of CL to the analysis of electron beam-sensitive materials and to depth-resolved analysis of metal–semiconductor interfaces[6] by using low electron-beam energies (on the order of 1 keV) will be extended to other materials and structures.

The continuing development of CL detection systems, cryogenic stages, and signal processing and image analysis methods will further motivate studies of a wide range of luminescent materials, including biological specimens.[12]

Related Articles in the Encyclopedia

EPMA, SEM, STEM, TEM, and PL

References

1 B. G. Yacobi and D. B. Holt. *Cathodoluminescence Microscopy of Inorganic Solids.* Plenum, 1990.

2 D. B. Wittry and D. F. Kyser. *J. Appl. Phys.* **38,** 375, 1967.

3 D. B. Holt. In: *Microscopy of Semiconducting Materials.* IOP, Bristol, 1981, p.165.

4 P. M. Petroff, D. V. Lang, J. L. Strudel, and R. A. Logan. In: *Scanning Electron Microscopy.* SEM Inc., Chicago, 1978, p. 325.

5 M. E. Hoenk and K. J. Vahala. *Rev. Sci. Instr.* **60,** 226, 1989.

6 L. J. Brillson and R. E. Viturro. *Scanning Microscopy.* **2,** 789, 1988.

7 C. E. Barker and T. Wood. In: *Process Mineralogy VI.* The Metallurgical Society of AIME, 1987, p. 159.

8 C. A. Warwick. *Scanning Microscopy* **1,** 51, 1987.

9 P. M. Petroff. In: *Microscopy of Semiconducting Materials.* IOP, Bristol, 1987, p.187.

10 B. G. Yacobi, S. Zemon, C. Jagannath, and P. Sheldon. *J. Cryst. Growth* **95,** 240, 1989.

11 A. T. Collins and S. C. Lawson. *J. Phys. Cond. Matter* **1,** 6929, 1989; L. H. Robins, L. P. Cook, E. N. Farabaugh, and A. Feldman. *Phys. Rev.* **B39,** 13367, 1989.

12 D. B. Holt. In: *Analysis of Organic and Biological Surfaces.* (P. Echlin, ed.) Wiley, New York, 1984, p.301.

3.4 STEM

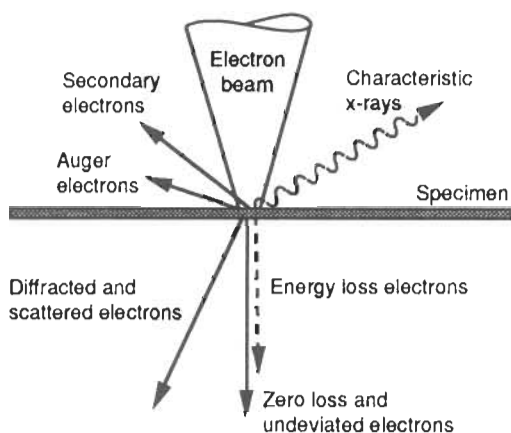## Scanning Transmission Electron Microscopy

CHARLES E. LYMAN

Contents

- Introduction
- Basic Principles
- Common Modes of Analysis and Examples
- Sample Requirements
- Artifacts
- Conclusions

Introduction

The Scanning Transmission Electron Microscope (STEM) produces images of the internal microstructure of thin specimens using a high-energy scanning electron beam, in the same way a Scanning Electron Microscope (SEM) produces images of bulk surfaces. The term STEM is also used to describe the group of crystallographic and compositional analysis methods known collectively as Analytical Electron Microscopy (AEM): Convergent Beam Electron Diffraction (CBED), X-ray microanalysis by Energy-Dispersive Spectrometry (EDS), and Electron Energy-Loss Spectrometry (EELS).[1-6] Many STEM images are similar to images from the Transmission Electron Microscope (TEM), and in certain modes the STEM is capable of resolving the atomic lattice of a solid and even single atoms on a thin support.

The STEM is unrivaled in its ability to obtain high-resolution imaging combined with microanalysis from specimens that can be fashioned from almost any solid. Major applications include the analysis of metals, ceramics, electronic devices

Figure 1 **Signals generated when the focussed electron beam interacts with a thin specimen in a scanning transmission electron microscope (STEM).**

and packaging, joining methods, coatings, composite materials, catalysts, minerals, and biological tissues.

There are three types of instruments that provide STEM imaging and analysis to various degrees: the TEM / STEM, in which a TEM instrument is modified to operate in STEM mode; the SEM/STEM, which is a SEM instrument with STEM imaging capabilities; and dedicated STEM instruments that are built expressly for STEM operation. The STEM modes of TEM / STEM and SEM / STEM instruments provide useful information to supplement the main TEM and SEM modes, but only the dedicated STEM with a field emission electron source can provide the highest resolution and elemental sensitivity.

Analysis capabilities in the STEM vary with the technique used. Crystallographic information may be obtained, including lattice parameters, Bravais lattice types, point groups, and space groups (in some cases), from crystal volumes on the order of 10^{-23} m^3 using CBED. Elemental identification and quantitative microanalysis have been developed for EDS and EELS. Detection limits for each technique are on the order of 0.1 wt % for one element combined with another. The EELS spectrum contains a rich variety of information concerning chemical bonding and dielectric constants in addition to elemental information. Since the STEM provides a through-section analysis (see Figure 1), it is complementary to surface techniques and should be used in conjunction with them. Also analytical signals may be collected as the small STEM electron probe scans across the specimen, providing compositional images in addition to the images typical of the SEM and the TEM. Compositional images showing elemental distributions have been obtained with spatial resolutions in the range 5–50 nm.
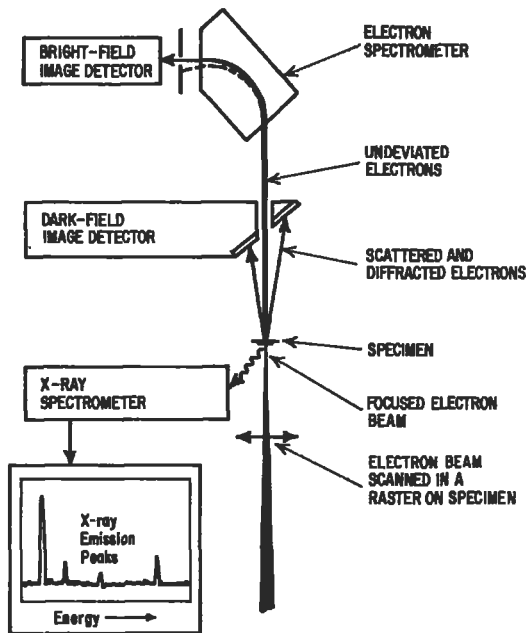
Figure 2 Schematic of a STEM instrument showing the principal signal detectors. The electron gun and lenses at the bottom of the figure are not shown.

The development of the STEM is relatively recent compared to the TEM and the SEM. Attempts were made to build a STEM instrument within 15 years after the invention of the electron microscope in 1932. However the modern STEM, which had to await the development of modern electronics and vacuum techniques, was developed by Albert Crewe and his coworkers at the University of Chicago.[7]

Basic Principles

Electron Probe Formation

An electron gun produces and accelerates the electron beam, which is reduced in diameter (demagnified) by one or more electromagnetic electron lenses. Electromagnetic scanning coils move this small electron probe (i.e., the beam) across the specimen in a raster. Electron detectors beyond the specimen collect a signal that is used to modulate the intensity on a cathode-ray tube that is scanned in synchronism with the beam on the specimen. A schematic of the essential components in a dedicated STEM system is shown in Figure 2.

The most important criterion for a STEM instrument is the amount of current in the small electron probe. Generally, 1 nA of probe current is required for high-

a   b
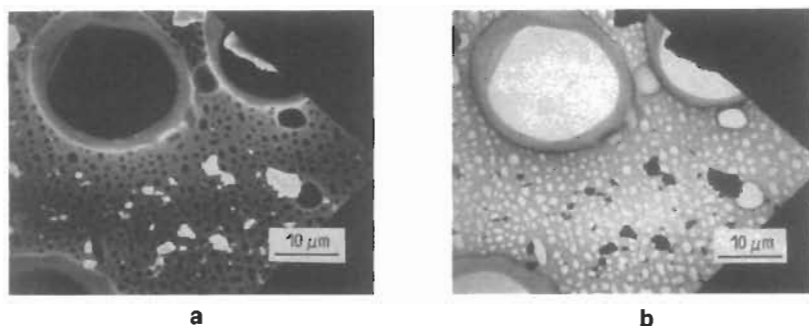
Figure 3   **Bright-field (a) and dark-field (b) STEM images of crushed ceramic particles dispersed on a "holey" carbon film supported on an electron microscope grid (shown at the right).**

quality microanalysis. For TEM/STEM and SEM/STEM systems using thermionic electron sources (tungsten wire or LaB_6), electron probes having diameters of 10–30 nm (measured as full width at half maximum) carry about 1 nA, and may be used for imaging and analysis. Smaller probes may be used for imaging, but the current may not be adequate for microanalysis. For the highest spatial resolution and analytical sensitivity, a STEM instrument with a field-emission electron gun must be used to provide 1 nA of current in an electron probe about 1–2 nm in diameter. These systems must use ultrahigh-vacuum technology at least in the electron gun, and preferably throughout the microscope.

Imaging

The scanning electron beam produces a diffraction pattern beyond the specimen similar to that formed in the TEM, and in most cases the image may be interpreted as mass–thickness contrast, diffraction contrast, or phase contrast. Bright-field images are formed by using an aperture to select only the undeviated transmitted beam from the diffraction pattern Figure 2, as in TEM (see the article on TEM). In STEM, the electron signal is collected with either a scintillator–photomultiplier or a semiconductor detector. Bright areas in the image indicate regions of the specimen that suffered little or no interaction with the electron beam (see Figure 3a). Dark-field images may be obtained in two ways: by selecting a single diffracted beam g_{hkl} to be collected on the detector; or by collecting all of the electrons diffracted or scattered beyond a certain minimum angle on an annular dark-field (ADF) electron detector. The former method gives images similar to the TEM dark-field images used for defect analysis in crystals (see the TEM article). The latter method provides a high-resolution, high-contrast image that is sensitive to specimen thickness and atomic number variations. Bright areas in the dark-field image

indicate regions of the specimen that are thick, strongly diffracting, or of high atomic number (see Figure 3b).

The detailed contrast in a STEM image, compared to a TEM image of the same specimen feature, depends on the incident electron beam convergence angle and the electron collection angle at the detector. The theorem of reciprocity states that if appropriate beam angles in TEM and STEM are made equivalent and the sample is inverted, then the STEM and TEM images of a thin specimen will be identical (see Cowley[1]). For example, if the STEM collection angle is reduced to a value typical of the TEM illumination angle, similar phase contrast lattice plane images and structure images may be observed in both STEM and TEM. Often, the STEM collection angle must be enlarged to provide an adequate signal level, which may alter the image contrast. Because of the scanning nature of image generation many other signals, such as secondary electrons and cathodoluminescence (light), also may be used for imaging.

Convergent Beam Electron Diffraction

When the electron beam impinging on the specimen has a high convergence angle (i.e., is in the form of a cone as shown in Figure 1), the electron diffraction pattern becomes an array of disks rather than an array of sharp spots as in TEM. The various manifestations of this type of electron diffraction pattern are known as Convergent Beam Electron Diffraction (CBED). The distance of each diffraction disk from the central beam may be calibrated to yield the interplanar *d*-value for a particular set of *hkl* planes. A diffraction disk containing no contrast detail is produced when a very thin region of a specimen (< 0.1 μm) is under the beam. Other than providing high spatial resolution (on the order of the electron beam size) this pattern of blank disks contains no more information than the typical selected area electron diffraction pattern (see the article on TEM).

Diffraction from thick crystals (0.1–0.5 μm) exhibits intensity variations within the disks caused by dynamical diffraction effects (see Steeds[1]). In this case the symmetry of the intensity variations provides information about the symmetry of the crystal that can be used as a "fingerprint" for phase identification.[8] Because the convergent electron beam senses the three-dimensional aspects of the specimen, CBED patterns from a crystal thicker than about 0.1 μm may be used to determine its point group, and often its space group.[9] If the magnification of the diffraction pattern is made very small and the convergence angle made very large so that the disks overlap, rings of intensity called *higher order Laue zone (HOLZ) rings* may be observed. These rings indicate that diffraction has occurred from other layers of the reciprocal lattice. If the crystal is tilted so that the beam is parallel to the [100], [010], and [001] crystal directions, the crystal lattice parameters along those directions may be determined. Also, fine details of a CBED pattern may yield a relative lattice parameter determination to better than 0.001 nm.

X-Ray Microanalysis

When energetic electrons bombard a solid, characteristic X rays from each element are generated that form the signal used in microanalysis. Characteristic X rays arise from de-excitation of atoms suffering inner-shell electron ionizations, and these X rays allow qualitative elemental identification and quantitative elemental composition determination. The X-ray signal is detected with an EDS placed close to the specimen inside the objective lens of the microscope (see the article on EDS). For materials science specimens, a quantification scheme for specific element pairs is well developed.[10] The ratio of elemental concentrations of two elements in the thin specimen may be determined by multiplying the X-ray intensity ratios of these elements by a sensitivity factor that depends only on the accelerating voltage and the X-ray detector configuration. When the elements in the specimen do not have large differences in their X-ray mass absorption coefficients, or when the specimen is very thin, corrections for X-ray absorption may be negligible and need not be applied to obtain an accuracy of 10–20% relative to the amount of element present. This modest level of analysis is still remarkable when it is realized that it may be obtained from regions of a specimen about 5 nm in diameter. To obtain quantitative results in the 5–10% range, an absorption correction should be applied using an estimate of the specimen thickness from CBED, EELS, or another method.[3–5] Using EDS methods, elemental detection is possible down to a few % wt. for elements having atomic numbers $Z < 11$ and down to 0.1–0.5 wt % for elements having $Z > 11$.

Microanalysis by Electron Energy-Loss Spectrometry

Electrons in the incident beam suffer inelastic collisions with atoms in the specimen; the effect of these collisions may be detected by measuring the energy of the primary electron after it has traversed the specimen. To observe a useful signal above background, very thin specimens (about 10–50 nm thick) must be used. Of the several inelastic events possible, the most useful for elemental analysis is the inner-shell ionization event that leads to characteristic X-ray and Auger electron emission. The shape of the spectrum at these characteristic inner-shell ionization energy losses is similar to the X-ray absorption edge. The signal intensity under the edge and above background can be related to the amount of the element in the specimen.[5] This microanalysis method is somewhat less accurate than EDS X-ray analysis because the ionization cross section, which is needed to convert the collected intensity to chemical composition, is often not well known. Details in the EELS spectrum reveal bonding information and information about the dielectric constant from regions of the specimen as small as 0.5 nm in diameter. Detection limits are similar to EDS, but the method is best applied to the K-edges for light elements from lithium to fluorine.
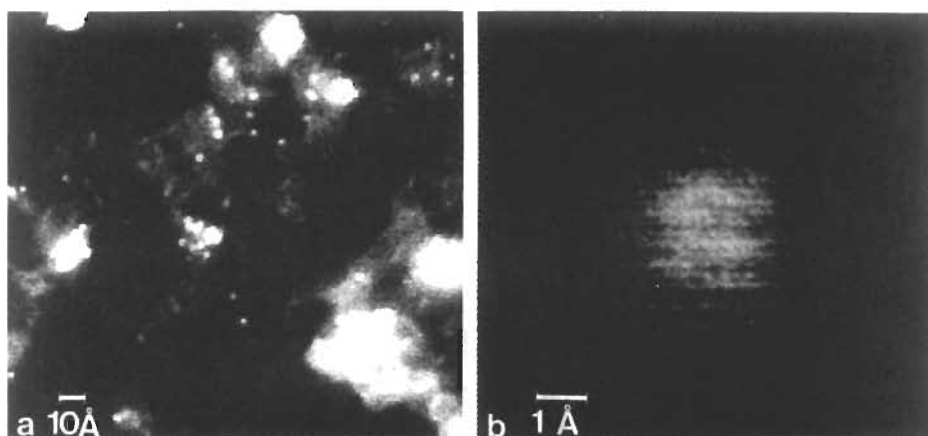
Figure 4 Annular dark-field STEM image of individual gold atoms on a very thin carbon film: (a) individual gold atoms appear as bright spots; and (b) higher magnification image showing a single gold atom. The scan lines are caused by the 0.25-nm electron beam traversing the gold atom about 15 times. (Courtesy of M. Isaacson)

Examples of Common Analysis Modes

The major STEM analysis modes are the imaging, diffraction, and microanalysis modes described above. Indeed, this instrument may be considered a miniature analytical chemistry laboratory inside an electron microscope. Specimens of unknown crystal structure and composition usually require a combination of two or more analysis modes for complete identification.

Conventional Bright-Field Imaging

Bright-field STEM images provide the same morphological and defect analysis typical of TEM images, such as particle sizing, interface analysis, and defect analysis (see Figure 3a). While the contrast may differ from TEM for thin crystalline materials, a dedicated STEM instrument using a field emission gun produces images that are similar enough to use the same image interpretation rationale developed for conventional TEM analysis.

Annular Dark-field Imaging

The annular dark-field detector of the field-emission STEM (see Figure 2) provides a powerful high-resolution imaging mode that is not available in the conventional TEM or TEM/STEM. In this mode, images of individual atoms may be obtained, as shown in Figure 4 (see Isaacson, Ohtsuki, and Utlaut[1]). Some annular dark-field
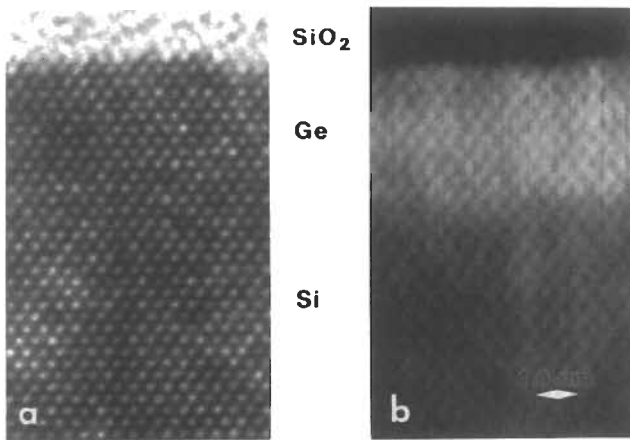
Figure 5   Images of a thin region of an epitaxial film of Ge on Si grown by oxidation of Ge-implanted Si: (a) conventional TEM phase contrast image with no compositional information; and (b) high-angle dark-field STEM image showing atomically sharp interface between Si and Ge. (Courtesy of S.J. Pennycook)

detectors have been modified to collect only the electrons that scatter into angles greater than 80 milliradians By collecting only the high-angle Rutherford-scattered electrons, images may be obtained that contain compositional information, as well as atomic-level image detail[11] (see Figure 5).

Point Group and Space Group Determination

Crystallographic structure determination is generally considered the realm of X-ray diffraction. However, three-dimensional sampling of the crystal by CBED allows first-principle determinations of point groups (crystal classes) for crystals as small as 100 nm, which could never be accomplished by X-ray methods. Figure 6 shows CBED patterns of a phase at the triple point of aluminum nitride grains containing Al, N, and O. These patterns helped to determine the point group and space group of this aluminum oxynitride spinel phase as m3m and Fd$\bar{3}$m, respectively.[12]

Microanalysis

Microanalysis of specimen regions in the nm-size range is one of the strongest reasons to use STEM. Figure 7 shows X-ray and EEL spectra taken simultaneously from the same area of a thin catalyst specimen. In each case the energy position of the peak or edge provides element identification, whereas the intensity above background for each peak and edge allows quantitative assessment of the composition. The statistics for these data are atypical owing to an intentionally short acquisition time of a few seconds. Figure 8a shows the statistics for a more typical X-ray spec-

a   b
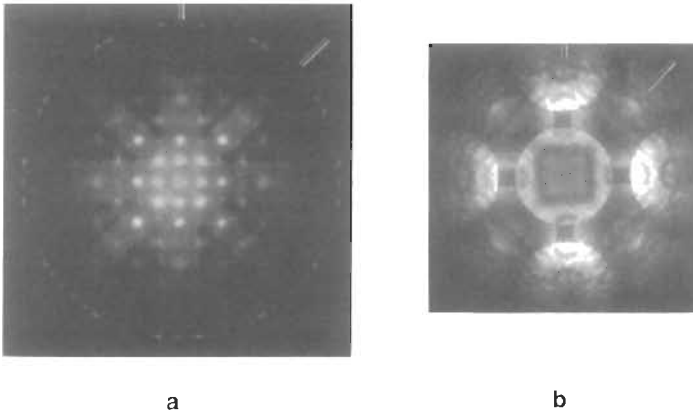
Figure 6   **CBED patterns of aluminum oxynitride spinel along the [001] direction. Sym-
metries in the patterns contributed to the determination of the point group
and space group: (a) whole pattern showing 1st Laue zone ring; and (b) 0th
order Laue zone. Both patterns show a fourfold rotation axis and two mirror
planes parallel to the axis. (Courtesy of V. P. Dravid)**

trum collected over 100 s. Note the low-energy carbon and oxygen peaks collected
with a windowless X-ray detector.

Phase Identification

Knowledge of the elements in an unknown phase, as determined by EDS or EELS,
usually does not permit identification of the compound. However, this elemental
information may be used in combination with interplanar spacing information
(*d*-values) from one or more CBED patterns (or even the SAD patterns mentioned
in the article on TEM) to render a positive identification. The task of searching all
inorganic compounds to make a positive identification is now easier because of a
new index to the JCPDS-ICDD Powder Diffraction File and the NIST Crystal
Data File called the *Elemental and Lattice Spacing Index*.[13] The elements deter-
mined from EDS or EELS analysis are used for the primary search, which places all
possible compounds on one or two pages for confirmation by matching to the ten
largest interplanar spacings listed for each entry.

Compositional Imaging

Elemental distributions in a thin specimen may be obtained at high resolution from
any properly prepared solid specimen using either EDS or EELS signals. These
images are sometimes called elemental maps. Elemental images usually collected
digitally by setting a region of interest in the spectrum for each element and storing
the counts collected in these windows as a function of electron beam position (stor-

a

X-Ray Energy (keV)

b

Electron Energy Loss (eV)
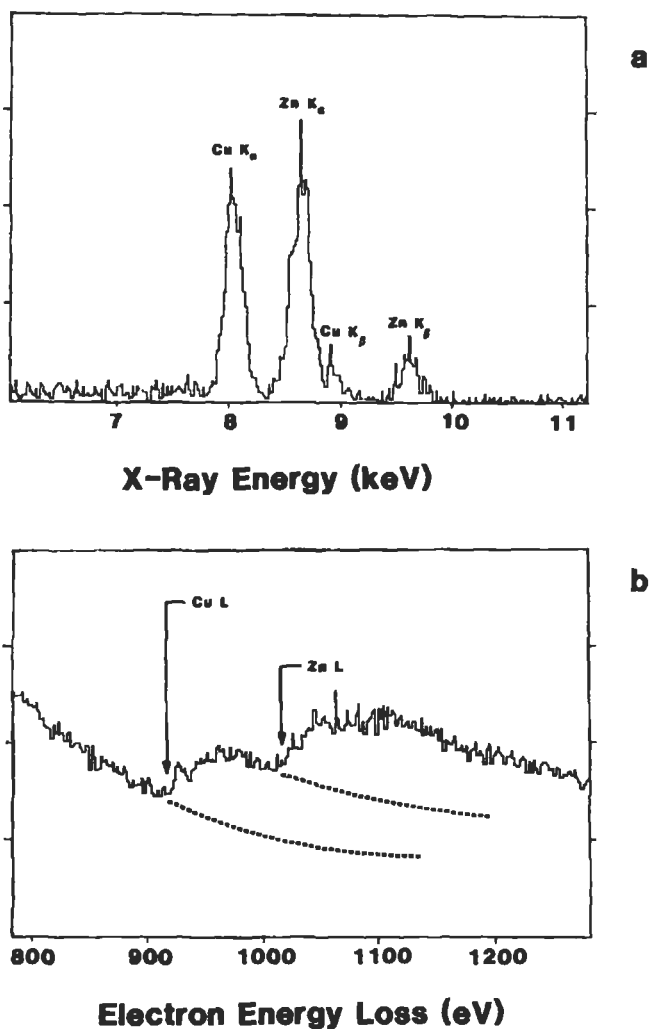
Figure 7   Microanalysis of a CuO/ZnO methanol synthesis catalyst with a field-emis-
sion STEM: (a) EDS data showing Cu and Zn K-lines; and (b) EELS data show-
ing Cu and Zn L-edges with dotted lines indicating background levels. Spectra
were taken simultaneously from a 2-nm diameter area. Signal intensities
above background show that approximately the same relative amounts of Cu
and Zn were measured by each method.

age at each image pixel), as shown in Figure 8b. An image of the X-ray background
signal was collected separately to determine that the distribution of sulfur in
Figure 8 is real.[14] Since the electron probe size is governed by the need for a large
probe current (about 1 nA), image magnification, pixel density, and counting time

a   b
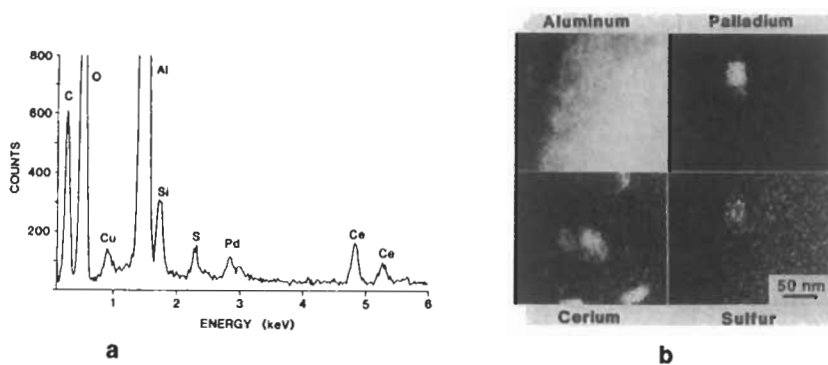
Figure 8   X-ray elemental imaging in a field-emission STEM: (a) EDS data of Pd / Ce / alumina catalyst particle poisoned with SO_2; and (b) 128 × 128 digital STEM images formed using X-ray counts collected at each image pixel for aluminum, palladium, cerium, and sulfur. (Courtesy of North-Holland Publishers)[14]

per pixel must be adjusted for the type of STEM instrument used. For example, if the pixel density is 128 × 128 with a counting time of 100 ms per pixel, a compositional image may be obtained in 28 min. However, for a thermionic source in a TEM–STEM system, where the counting time per pixel must be increased to 3 s per pixel, the total frame time for a similar image is about 14 hours. When elements are present in high concentration (>20 wt %), the resolution of the X-ray elemental image can be < 5 nm. Elemental images using EELS signals can be of even higher resolution, although more computation is necessary to subtract the background.

Sample Requirements

Specimens suitable for imaging in TEM are usually acceptable for STEM imaging and analysis. The principal methods for producing suitable thin specimens are electropolishing (metals only), ion-beam thinning (all hard materials), and ultramicrotomy (polymers, some metals, and small hard particles).[15] In the first two cases the specimen is thinned to perforation, and analysis takes place around the edge of the hole. Ultramicrotomed specimens are relatively uniform in thickness, but the fragile thin sections must be supported by a specimen grid. Hard, brittle materials also may be crushed to a powder and dispersed on a carbon film supported on a specimen grid, as in Figure 3. For microscopy of layered materials it is useful to dice the specimen to reveal a cross section of the layers before ion-beam milling. Precipitates in a metal matrix may be extracted using the extraction replica technique.

Microanalysis often places special constraints on the preparation of thin specimens beyond the general requirement to be transparent to 100-keV electrons.

CBED usually requires analysis along a particular crystallographic direction, and although specimen-tilting facilities are available in the microscope, often it is useful to orient the specimen before specimen preparation so that the thinned direction is along a crystal direction of interest. For high-quality microanalysis by EDS or EELS, the thin specimen must be free of surface films containing elements redistributed from the bulk or from contamination sources that would change the measured through-section composition. Ion-beam milling for short times usually removes such films deposited by electropolishing; however, ion-beam milling for long times may introduce elemental redistribution by differential sputtering. Specimens prepared by ultramicrotomy, extraction replication, or crushing generally do not have these compositional artifacts. Occasionally microanalysis is performed on specimens prepared by one of the latter methods while images of the same material might be obtained from electropolished or ion-beam milled specimens.

Artifacts

The major artifact typical of STEM imaging is a buildup of hydrocarbon contamination under the electron beam. This contamination appears in the bright-field image as a dark area in the shape of the scanning raster or as a dark spot if the beam has been stopped for microanalysis. Besides obscuring features in the image, contamination layers can absorb X rays from the lighter elements and increase the background in EELS analysis. Contamination can be reduced by heating the specimen in vacuum before examination, by cooling the specimen during analysis, and by improving the vacuum in the specimen chamber to better than 10^{-6} Pa (about 10^{-8} torr).

In addition to cleanliness (contamination effects), surface morphology and the alteration of composition during specimen preparation can cause serious artifacts in microanalysis. In some older instruments, the microscope itself produces undesirable high-energy X rays that excite the entire specimen, making difficult the accurate quantitation of locally changing composition. Artifacts also are observed in the EDS X-ray spectrum itself (see the article on EDS).

Conclusions

STEM can provide image resolution of thin specimens rivaling TEM, but in addition can provide simultaneous crystallographic and compositional analysis at a higher spatial resolution than any other widely-used technique. Any solid material may be examined, provided that a specimen can be prepared that is less than about 100 nm in thickness.

Future developments of this instrumentation include field emission electron sources at 200–300 kV that will allow better elemental detectability and better spatial resolution. Multiple X-ray detectors having large collection angles will also improve elemental detectability in X-ray microanalysis. The higher accelerating

voltages should allow EDS X-ray and EELS compositional measurements to be made on specimens of the same thickness, instead of requiring a much thinner specimen for EELS. Electronic capture of digital diffraction pattern images should make some automation of diffraction pattern analysis possible. Under complete digital control automated experiments will be possible that cannot be accomplished manually.

Related Articles in the Encyclopedia

TEM, EDS, EELS, and SEM

References

1 *Introduction to Analytical Electron Microscopy.* (J. J. Hren, J. I. Goldstein, and D. C. Joy, eds.) Plenum, New York, 1979. Somewhat dated text that is still useful for certain chapters including those of Cowley, Steeds, and Isaacson, et al.

2 *Quantitative Microanalysis with High Spatial Resolution.* (G. W. Lorimer, M. H. Jacobs, and P. Doig, eds.) The Metals Society, London, 1981. Research papers giving results from many materials.

3 D. B. Williams. *Practical Analytical Electron Microscopy in Materials Science.* Philips Electronic Instruments, Mahwah, NJ, 1984. Concise textbook on CBED, EDS, and EELS with a pronounced "how-to" flavor.

4 *Principles of Analytical Electron Microscopy.* (D. C. Joy, A. D. Romig Jr, and J. I. Goldstein, eds.) Plenum, New York, 1986. An updated version of Reference. 1.

5 R. F. Egerton. *Electron Energy Loss Spectroscopy in the Electron Microscope.* Plenum, New York, 1986. The principle textbook on EELS.

6 *High Resolution Transmission Electron Microscopy and Associated Techniques.* (P. R. Buseck, J. M. Cowley, and L. Eyring, eds.) Oxford University Press, New York, 1988. A review covering these techniques in detail (except X-ray microanalysis) including extensive material on high-resolution TEM.

7 A. V. Crewe, J. Wall, and J. Langmore. *Science.* **168,** 1338, 1970. The classic first attempt to image single atoms with the STEM.

8 J. Mansfield. *Convergent Beam Electron Diffraction of Alloy Phases.* (by the Bristol Group, under the direction of J. Steeds, and compiled by J. Mansfield) Hilger, Bristol, 1984. This book is an atlas of CBED patterns that may be used to identify phases by comparing published patterns with experimental patterns.

9 B. F. Buxton, J. A. Eades, J. A. Steeds, and G. M. Rackham. *Phil. Trans. R. Soc. A.* **281,** 171, 1976. This paper outlined point group determination for the first time, but the major conclusions are also summarized in Williams (*op. cit.*).

10 G. Cliff and G. W. Lorimer. *J. Microscopy.* **103,** 203, 1975. This paper summarizes the Cliff-Lorimer analysis technique, but more complete reviews of the method may be found in References 1–4.

11 S. J. Pennycook. *EMSA Bulletin.* **19,** 67, 1989. A summary of compositional imaging using a high-angle annular dark-field detector in a field emission STEM instrument published by the Electron Microscopy Society of America, Box EMSA Woods Hole, MA 02543.

12 V. P. Dravid, J. A. Sutliff, A. D. Westwood, M. R. Notis, and C. E. Lyman. *Phil. Mag. A.* **61,** 417, 1990. An example of how to practically determine the space group of a phase.

13 *JCPDS-ICDD Elemental and Lattice Spacing Index* (1990). This index is available from JCPDS-International Centre for Diffraction Data, 1601 Park Lane Swarthmore, PA 19081.

14 C. E. Lyman, H. G. Stenger, and J. R. Michael. *Ultramicroscopy.* **22,** 129, 1987. This paper demonstrates high-resolution compositional imaging with the field-emission STEM.

15 *Specimen Preparation for Transmission Electron Microscopy of Materials* (J. C. Brauman, R. M. Anderson, and M. L. McDonald, eds.) MRS Symp. Proc vol. 115, Materials Research Society, Pittsburg, 1988. This conference proceedings contains many up-to-date methods as well as references to books on various aspects of specimen preparation.

3.5   EPMA

Electron Probe X-Ray Microanalysis[1]

DALE E. NEWBURY

Contents

- Introduction
- Physical Basis of EPMA
- Measurement of X-Rays
- Qualitative Analysis
- Quantitative Analysis
- Compositional Mapping
- Conclusions

Introduction

Electron Probe X-Ray Microanalysis (EPMA) is a spatially resolved, quantitative elemental analysis technique based on the generation of characteristic X rays by a focused beam of energetic electrons.[1-3] EPMA is used to measure the concentrations of elements (beryllium to the actinides) at levels as low as 100 parts per million (ppm) and to determine lateral distributions by mapping. The modern EPMA instrument consists of several key components:

1   An electron-optical column capable of forming a beam ranging in diameter from nm to μm and carrying a current ranging from pA to μA

2   An energy-dispersive X-ray spectrometer and at least one wavelength-dispersive X-ray spectrometer

3   An optical microscope for precise positioning of the specimen relative to the X-ray spectrometers

4   A vacuum system capable of operating at pressures ranging from 10^{-4} to 10^{-6} Pa

1. Note: This artcle is a contribution of the United States Government and is not subject to copyright.
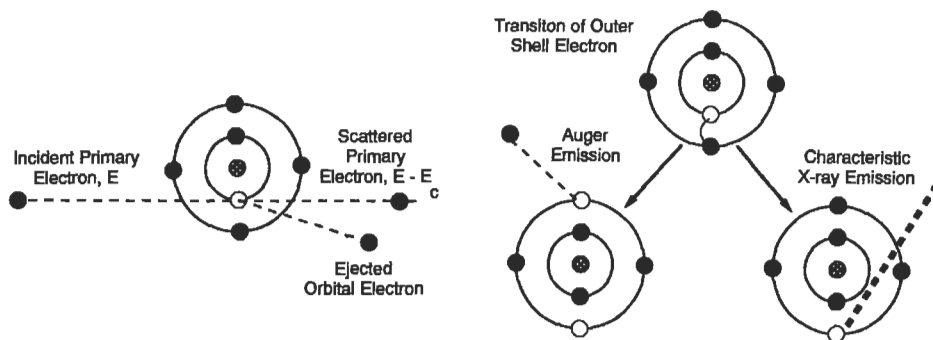
Figure 1   **Schematic of inner shell ionization and subsequent deexcitation by the Auger effect and by X-ray emission.**

5 A computer system to control the beam, spectrometers, specimen stage, and quantitative data processing.

The electron-optical performance of the EPMA system is indistinguishable from that of a conventional scanning electron microscope (SEM); thus, EPMA combines all of the imaging capabilities of a SEM with quantitative elemental analysis using both energy- and wavelength-dispersive X-ray spectrometry.[2, 3]

Physical Basis of EPMA

The physical basis of electron probe microanalysis is the generation of characteristic X rays by bombarding a solid with energetic electrons. Interactions of energetic electrons with matter include elastic scattering, which causes significant angular deviation of the electron trajectories, and inelastic scattering, which reduces the energy of the electrons and sets a limit to their range. Mechanisms of inelastic scattering include the production of secondary electrons, inner shell ionization, bremsstrahlung (continuum) X rays, long-wavelength electromagnetic radiation in the ultraviolet, visible, and infrared regions, electron–hole pairs, lattice vibrations (phonons), and electron oscillations (plasmons). The rate of energy loss depends on the electron energy and the target composition, and is typically 0.1–10 eV/nm. Inner shell ionization, illustrated in Figure 1, occurs when the beam electron ejects a bound atomic electron by transferring sufficient energy to the atom to exceed the critical excitation (or binding) energy E_c of an atomic electron. The resulting atomic vacancy is filled by a transition involving one or more outer shell electrons. The energy difference between shell levels can be manifested as an emitted X-ray photon, or the energy can be transferred to another outer shell electron, which is ejected as an Auger electron. Because the energy of the atomic shells is sharply defined, the emitted X ray or Auger electron has a precisely defined energy and is therefore characteristic of the atom species originally ionized by the beam electron.

For atoms having an atomic number greater than 10, the electron filling the inner shell vacancy may come from one of several possible subshells, each at a different energy, resulting in families of characteristic X-ray energies, e.g., the $K\alpha$, β family, the $L\alpha$, β, γ family, etc.

The beam electrons also produce X rays when they undergo deceleration in the Coulombic field of the specimen atoms, losing energy and emitting X rays known as "braking" radiation, or *bremsstrahlung*. Since this energy loss can take on any value from 0 to the entire energy carried by the high-energy electron, the bremsstrahlung X rays form a continuum background spanning all energies. Bremsstrahlung X rays are indistinguishable from characteristic X rays that may occur at the same energy. Statistical fluctuations in this bremsstrahlung background form the eventual limit that determines the ultimate sensitivity of electron probe X-ray microanalysis.

The critical parameter for X-ray generation is the overvoltage $U = E_0/E_c$, where E_0 is the incident beam energy. The intensity of characteristic X rays is given by:

$$I_{ch} = a i_B (U - 1)^n \tag{1}$$

where a is a constant, i_B is the beam current, and the exponent n is approximately 1.5.

Equation (1) demonstrates that the analyst must choose a beam energy that exceeds the critical excitation energy for the species to be analyzed. In general, a value of $U > 2$ is required to achieve adequate efficiency in the production of X rays.

The volume of analysis, i.e., the diameter and depth of the analyzed region, is limited by a combination of the elastic and inelastic scattering. The maximum depth of the interaction volume is described by the Kanaya-Okayama electron range:

$$R(\mu m) = \left(\frac{0.0276A}{Z^{0.89}\rho} \right) E_0^{1.67} \tag{2}$$

where Z is the atomic number, A is the atomic weight (g/mole), ρ is the density (g/cm^3), and E_0 is the incident beam energy (keV). The maximum width of the interaction volume is similar in value to the range. When the production of X rays is considered, the range is reduced because X rays for a particular element cannot be produced below E_c for that element. Equation (2) is modified to reflect this condition:

$$R_X(\mu m) = \left(\frac{0.0276A}{Z^{0.89}\rho} \right) (E_0^{1.67} - E_c^{1.67}) \tag{3}$$

Monte Carlo electron trajectory simulations provide a pictorial view of the complex electron–specimen interaction. As shown in Figure 2a, which depicts the interac-
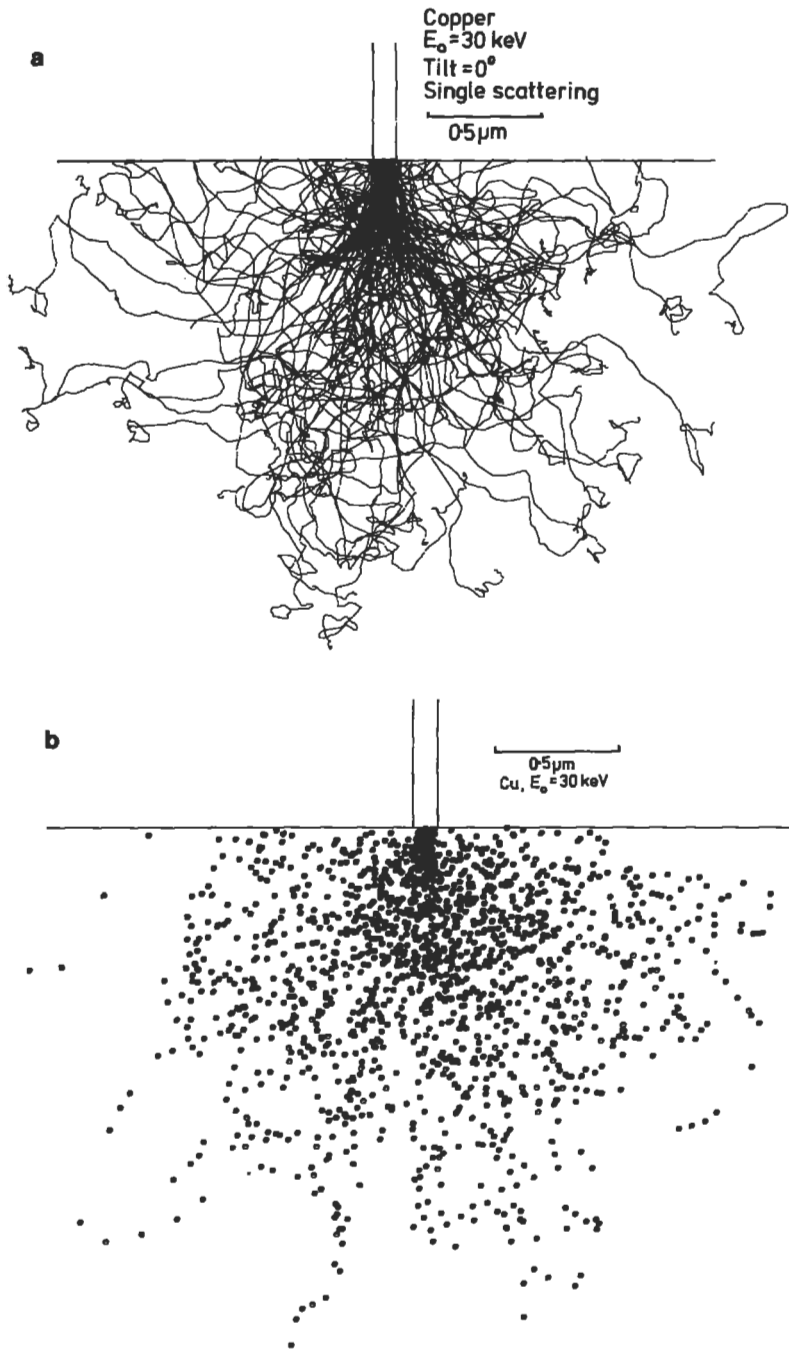
Figure 2 (a) Monte Carlo simulation of electron trajectories in copper, beam energy 30 keV. (b) Corresponding sites of K-shell ionization.
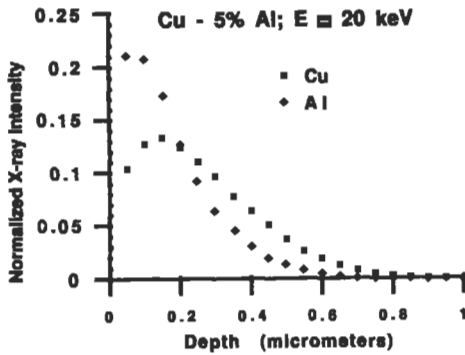
Figure 3 Depth distribution of generation of Cu Kα X rays for an incident beam energy of 20 keV, and the effect of absorption.

tion volume of a beam incident perpendicularly on a flat specimen of copper, the interaction volume has dimensions on the order of μm. Generally, the spread of the electrons through the specimen, not the diameter of the incident probe, is the limiting factor in determining the spatial resolution of analysis. A focused beam carrying sufficient electron current for analysis can be obtained with a diameter that is generally a factor of 5–10 smaller than the dimension of the interaction volume given by Equation (3). For example, the range for production of Cu Kα X rays at an incident beam energy of 20 keV in copper is approximately 1 μm, while a beam diameter of 100 nm (0.1 μm) would carry sufficient beam current for analysis. The production of X rays within the interaction volume is illustrated in Figure 2b. An important concept related to the interaction volume is the depth distribution of X rays, the so-called $\phi(\rho z)$ function shown in Figure 3. This function forms the basis for the development of matrix correction procedures in the quantitative analysis protocol described below.

Measurement of X Rays

The analyst has two practical means of measuring the energy distribution of X rays emitted from the specimen: energy-dispersive spectrometry and wavelength dispersive spectrometry. These two spectrometers are highly complementary; the strengths of each compensate for the weaknesses of the other, and a well-equipped electron probe instrument will have both spectrometers.

Energy Spectrometry (EDS) uses the photoelectric absorption of the X ray in a semiconductor crystal (silicon or germanium), with proportional conversion of the X-ray energy into charge through inelastic scattering of the photoelectron. The quantity of charge is measured by a sophisticated electronic circuit linked with a computer-based multichannel analyzer to collect the data. The EDS instrument is

purely a line-of-sight device; any X ray emitted from the specimen into its solid angle of collection can be measured. To reduce thermal noise, the detector crystal and preamplifier are cooled to liquid nitrogen temperatures. For application to conventional electron-optical columns with a pressure on the order of 10^{-4} Pa, a thin window of beryllium, diamond, boron carbide, or a metal-coated polymer is used to protect the crystal from condensing water vapor from the microscope environment. The window material, the gold surface electrode, and an inevitable "dead layer" of partially active semiconductor just below the electrode act to absorb X rays. With optimum low-mass window materials like diamond or boron carbide, the EDS can measure X rays as low in energy as the Be K level (0.109 keV).

Wavelength Spectrometry (WDS) is based upon the phenomenon of Bragg diffraction of X rays incident on a crystal. The diffraction phenomenon is described by the expression:

$$n\lambda = 2d\sin\theta_B \tag{4}$$

where λ is the wavelength equivalent of the X-ray energy E: λ (nm) = 1.2398/E (keV), d is the crystal spacing for the diffracting planes; and θ_B is the angle at which constructive interference occurs (i.e., the Bragg angle). The WDS instrument is mechanical in nature and is a focusing device (see Figure 1). The X-ray source at the specimen, the diffracting crystal, and the gas counter to detect the X rays must follow a specific geometry (a Rowland circle) to satisfy Equation (4); accurate positioning is ensured by incorporating an optical microscope into the electron probe. To detect a wide energy range, different crystals with various d spacings are mounted on a mechanical turret, and are selectable under computer control.

EDS and WDS spectra of a multielement glass, shown in Figure 4, illustrate some major strengths and weaknesses:

1   Spectral acquisition. An EDS instrument can measure any X-ray photon that reaches the detector, and thus can continuously view the entire X-ray spectrum (0.1–20 keV), while the WDS instrument must be mechanically scanned with several crystal changes to acquire a complete spectrum over that same range. In Figure 4, for equivalent sensitivity, the WDS spectrum required approximately a factor of 10 greater acquisition time. When an unknown is examined, it is highly unlikely that a complete qualitative WDS scan will be made at every location chosen for analysis. Since EDS is always capable of measuring a complete spectrum, unexpected major and minor constituents can always be detected. For survey work of major and minor constituents in unknowns, EDS therefore has a significant advantage for rapid qualitative analysis.

2   Spectral resolution. Consider a Mn Kα photon, which has a natural peak width (the full width at half maximum, or FWHM) of approximately 1
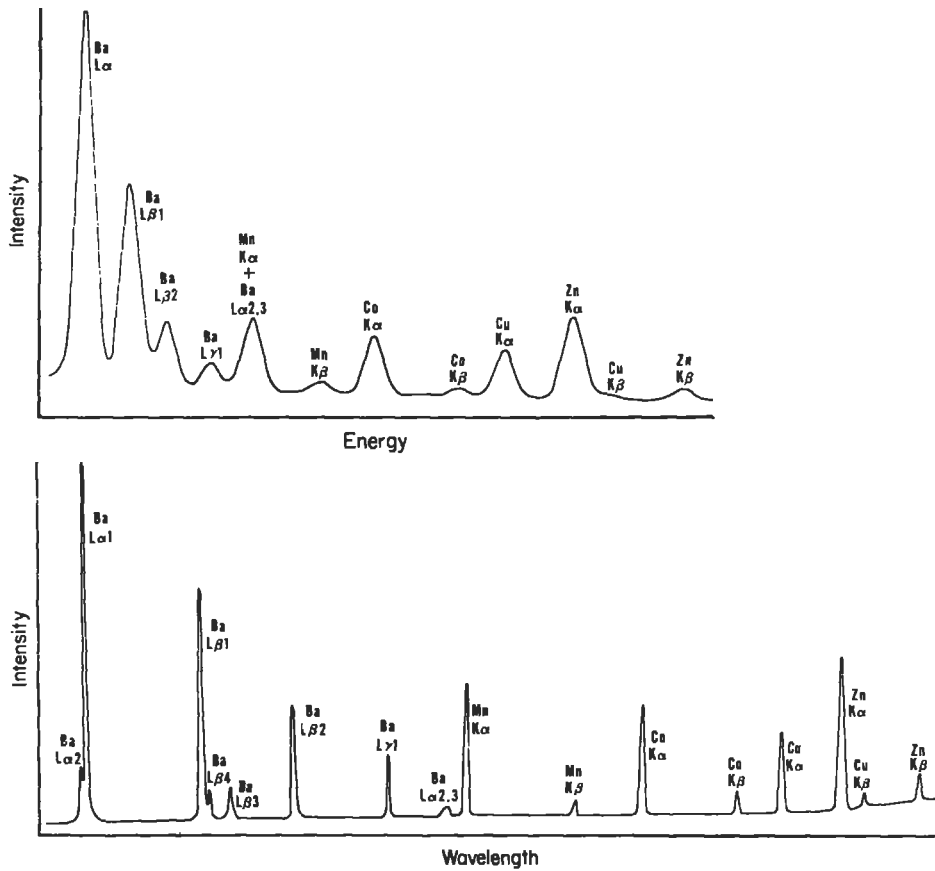
Figure 4 Comparison of EDS and WDS spectra from a complex, multielement glass. (Courtesy of Charles Fiori, National Institute of Standards and Technology)

eV. In WDS, the diffraction process, diffraction crystal imperfections, and the mechanical construction degrade this peak to a FWHM of approximately 10 eV. In EDS, the statistics of charge carrier creation degrade the peak to a FWHM of approximately 140 eV. The effect of spectral resolution can be seen readily in Figure 4, where a single peak in the EDS spectrum is actually composed of Mn Kα (keV) + Ba L$\alpha_{2, 3}$. This double peak is easily resolved using WDS into two peaks that differ in relative intensity by a factor of 10. Although powerful methods for mathematical spectral deconvolution of peaks can be applied to EDS spectra, deconvolution is likely to produce false solutions when the peaks are separated by less than 50 eV, when the peaks are sharply different in relative intensity, and when

significant statistical fluctuations exist in the spectral data, which is usually the situation in practical analysis. A classic example of an EDS interference situation encountered in practical analysis is that of S Kα, β (2.307 keV), Mo Lα, β (2.29 keV), and Pb Mα, β (2.346 keV); this interference situation is easily resolved by WDS.

3   Peak-to-background ratio and limits of detection. The peak-to-background ratio, which is a direct consequence of the spectral resolution, plays a major role in determining the limits of detection. A peak is more sharply defined with WDS than with EDS. The peak-to-background ratio is proportionally higher, since the intensity due to the characteristic radiation is spread over a smaller energy range of the X-ray continuum background. In practical analysis situations, the limit of detection for WDS is 100 ppm while that for EDS is approximately 0.1% wt. (1000 ppm) for elements having an atomic number > 11 (sodium). The detection limits are substantially poorer for light elements because of the high absorption losses in the specimen and spectrometer components. Depending on the matrix, the detection limit for light elements may be as high as 1–10% wt.

4   Dead time and limiting count rate. The pulse-processing time (dead time) is on the order of 10–50 μs for EDS and 0.5–1 μs for WDS. Because the WDS makes use of the diffraction effect to disperse the X rays before the detector, the limiting count rate applies to a single X-ray peak of interest; limiting count rates of 10^5 cps are possible and trace constituents can be measured with no dead time from major constituent peaks. The EDS instrument, which has a limiting count rate of approximately 2.5×10^4 cps, must process every X-ray photon in the range from the low-energy cutoff (approximately 100 eV) to the beam energy. The EDS dead time applies to the total spectrum rather than to a single peak of interest, making trace constituent measurement much more difficult.

5   Spectrometer positioning. The WDS instrument is a focusing optical device, with an ellipsoid of volume in focus for uniform X-ray transmission. The long axes of the ellipsoid have dimensions on the order of 100 to 1000 μm, while the short axis is approximately 10 μm. Precise positioning is vital if consistent X-ray intensity measurements are to be obtained. On a formal electron probe, this positioning is ensured by incorporating an optical microscope with its shallow depth of field and mechanically translating the specimen stage. The EDS instrument is a nonfocusing device, and it is therefore not critical to position it accurately relative to the specimen.

Qualitative Analysis

Qualitative analysis is generally assumed to be a trivial procedure consisting of matching the observed peaks to tabulated energies. Identification of peaks of major constituents is possible with a high degree of confidence, but misidentification of low-intensity peaks from minor and trace constituents is very much a possibility unless a careful strategy is followed. A good qualitative analysis strategy consists of first identifying the principal peaks of a major constituent and then locating all associated low-intensity peaks, including other X-ray family members, as well as all spectral artifacts, such as escape and sum peaks for EDS; for WDS, multiple-order lines—n = 2, 3, 4, etc., in Equation (4)—and satellite lines must be located. Only then should remaining peaks be identified as minor and trace constituents. Generally, the confidence with which a minor or trace constituent can be identified will be reduced because fewer peaks can be recognized above background. Absolutely no spectral smoothing should be applied in EDS spectra, since this introduces false "peaks" due to statistical fluctuations.

Quantitative Analysis

The keystone of practical quantitative electron probe microanalysis is Castaing's first approximation, which relates the concentration for a constituent in the unknown to the concentration in a standard in terms of the ratio of X-ray intensities generated in the target:[1]

$$\frac{C_i}{C_i^*} \sim \frac{I_i^G}{I_i^{*G}} \tag{5}$$

where C is the mass concentration, I^G is the generated characteristic peak intensity (corrected for dead time, peak overlaps, and background), i denotes a specific constituent, and * denotes the standard, such as a pure element. What is actually measured is the ratio of emitted intensities I_i^E / I_i^{*E}, the so-called k value. The emitted X-ray intensity ratio deviates from the generated intensity ratio in Equation (5) because of interelement or matrix effects; that is, the intensity of element i is affected by the presence of other elements j, k, l, etc., in the specimen. The origin of these matrix effects can be obtained by examining Figures 2 and 3.

Matrix Corrections

Atomic Number Effect

A significant fraction—about 15% for aluminum, 30% for copper, and 50% for gold—of the beam electron trajectories intersect the surface and escape as backscattered electrons (BSEs), as shown in Figure 2a. The majority of BSEs escape with more than half of their incident energy. Clearly, if these electrons had remained in

the specimen, they would have continued to scatter inelastically to produce additional X rays; their loss reduces the total possible generated intensity. The X-ray loss due to backscattering depends strongly on the specimen's composition, and increases with average atomic number. A related effect concerns the stopping power, or rate of energy loss, of the electrons within the specimen, which is also composition dependent.

Absorption Effect

Figures 2b and 3 demonstrate that X rays are produced over a range of depth into the sample. The X rays must propagate along a finite path through the specimen to reach the detector, and are subject to photoelectric absorption and scattering, which follows an exponential relation:

$$\frac{I}{I_0} = \exp\left[\left(\frac{-\mu}{\rho}\right) \rho z \csc \psi \right] \tag{6}$$

where I is the X-ray intensity; μ/ρ is the mass absorption coefficient (cm^2/g), which depends on composition; z is the depth below the surface (cm); and ψ is the detector take-off angle, which is the angle between the detector's axis and the specimen's surface. Figure 3 shows the distribution of X-ray production with depth that escapes the specimen for Cu Kα and Al Kα in a 90% copper–10% aluminum alloy. Although the Al Kα X ray is actually produced deeper in the specimen according to Equation (3), self absorption of the X rays by the specimen limits the sampling depth to be less than that for Cu Kα X rays. The sampling depths are quite different for Cu Kα and Al Kα in this case because of the difference in the mass absorption coefficients. Note that the absorption effect becomes greater as the X rays are produced deeper in the specimen, which provides another reason to operate at the lowest practical beam energy to minimize the range of the electrons.

Fluorescence Effect

A consequence of absorption of X rays is the inner shell ionization of the absorbing atoms and the subsequent generation of characteristic X rays from the absorbing atoms, called secondary fluorescence, which raises the generated intensity over that produced by the direct action of the beam electrons. Secondary fluorescence can be induced by both characteristic and bremsstrahlung X rays. Both effects are compositionally dependent.

Quantitative Calculations

Fortunately, the physics of interaction of energetic electrons and X rays with solid matter is sufficiently well understood to permit implementation of a quantitative analysis procedure, the so-called ZAF method, which is based upon a combination of theory and empiricism, to calculate separate correction factors for each of the

matrix effects. Each factor—atomic number Z, absorption A, and fluorescence F—is calculated as a ratio for the postulated specimen composition compared to the known composition of the standard. These factors multiply the measured k value to give a concentration ratio:

$$C_i = ZAF\left(\frac{I_i^E}{I_{i^*}^E}\right)C_{i^*} \tag{7}$$

Since the composition of the unknown appears in each of the correction factors, it is necessary to make an initial estimate of the composition (taken as the measured k value normalized by the sum of all k values), predict new k values from the composition and the ZAF correction factors, and iterate, testing the measured k values and the calculated k values for convergence. A closely related procedure to the ZAF method is the so-called $\phi(\rho z)$ method, which uses an analytic description of the X-ray depth distribution function determined from experimental measurements to provide a basis for calculating matrix correction factors.

A particular strength of Equation (7) is that the intensity ratio is formed between measurements of the same X-ray energy in both the unknown and standard. This procedure has significant advantages: First, there is no need to know the spectrometer's efficiency, a value that is very difficult to calibrate absolutely, since it appears as a multiplicative factor in both terms and therefore cancels. Second, an exact knowledge of the inner shell ionization cross section or fluorescence yields is not needed, since they also cancel in the ratio.

Accuracy of Electron Probe Microanalysis

Experience gained in the ZAF analysis of major and minor constituents in multielement standards analyzed against pure element standards has produced detailed error distribution histograms for quantitative EPMA. The error distribution is a normal distribution centered about 0%, with a standard deviation of approximately 2% relative. Errors as high as 10% relative are rarely encountered. There are several important caveats that must be observed to achieve errors that can be expected to lie within this distribution:

1 The characteristic peaks must be separated from the background. In EDS this is usually accomplished by mathematical filtering of the spectrum or by background modeling. In WDS, the peak is sufficiently sharp to permit background measurement by detuning the spectrometer.

2 The characteristic peaks must be deconvolved to eliminate peak interference; powerful deconvolution algorithms exist for EDS and WDS.

3 The unknown and standards must be measured under identical conditions of beam energy and spectrometer parameters. The specimen's surface must be oriented to known angles relative to the electron beam and the detector. All meas-

urements must be normalized to the same electron dose.

4 Differences in the specimen composition relative to the standard are the only source of difference in the measured X-ray intensities. There are no specimen size or shape effects influencing the electron–X-ray interactions, as in the case of particles or rough surfaces. To ensure this, the specimen must be flat and mirror-polished, with fine-scale surface topography reduced to less than 2% of the dimensions of the interaction volume. The specimen must be of sufficient thickness, typically > 50 μm, to contain the electron-excited volume as well as the full range of X-ray induced secondary fluorescence. No chemical polishing or etching can be tolerated because of the danger of modifying the near-surface composition through selective leaching.

5 The specimen must be homogeneous throughout the interaction volume sampled by the beam, since X rays of different energies originate from different depths.

6 The atomic number of the analyzed species must be 11 (sodium) or higher. For light elements from beryllium to fluorine, the low energy of the characteristic X rays leads to high absorption situations and an absorption correction factor exceeding 2. The mass absorption coefficients for the X rays of these elements are poorly known, so that large relative errors exceeding 10% are often encountered. Consequently, in fully oxidized systems, oxygen is frequently calculated indirectly by means of assumed stoichiometry for the cation species.

7 If all constituents are separately measured, or are calculated by stoichiometry, as in the case of oxygen, then the analytical total, which is the sum of all elements plus any calculated by stoichiometry, conveys useful information. If the analytical total is above 102%, a possible mistake in the measurement of the electron dose or an unexpected change in spectrometer parameters is likely. If the analytical total is significantly below 98%, an additional constituent is likely to have been missed.

When multielement standards similar in composition to the unknown are available, a purely empirical mathematical procedure, the Bence-Albee or Ziebold-Ogilvie method, can be applied. This procedure is often used in the analysis of minerals for which close standards exist.

The "standardless" approach attempts to apply first principles descriptions of X-ray production to the calculation of interelement relative sensitivities. Several of the key parameters necessary for first principles calculations are poorly known, and the accuracy of the standardless method often suffers when different X-ray families must be used in measuring several elemental constituents in a specimen.

Special Cases of Quantitative Analysis

Particles, rough surfaces, inclusions, layered film materials, and films on substrates represent special cases of considerable technological importance where the conventional quantitative analysis procedures fail. In such materials, shape and dimensions can influence the interaction of the beam electrons and the production of X rays. Several different strategies have been developed for dealing successfully with such geometric effects.[2, 3] These methods range from simple approaches, such as normalization of the analytical total to compensate for particle effects, to complex mathematical treatments, including theoretical or empirical modifications of the ZAF correction factors and rigorous Monte Carlo electron trajectory simulation of the exact geometrical boundary conditions of the specimen. Films on substrates, including multilayers, can be analyzed with corrections calculated by the $\phi(\rho z)$ method.[5] For particles and rough surfaces, errors in excess of 100% relative may be encountered with calculations uncorrected for geometrical effects; with simple normalization the maximum errors will generally be less than 25% relative. When the feature of interest is an inclusion contained in a matrix of different composition, where the lateral and depth dimensions of the inclusion are less than the X-ray range, quantitative and even meaningful qualitative analysis becomes impossible, since the interaction volume simultaneously samples both the inclusion and the surrounding matrix. In such cases, it may be necessary to mechanically or chemically separate the inclusions, and to analyze them as freestanding particles.

Compositional Mapping

Because X-ray counting rates are relatively low, it typically requires 100 seconds or more to accumulate adequate counting statistics for a quantitative analysis. As a result, the usual strategy in applying electron probe microanalysis is to make quantitative measurements at a limited collection of points. Specific analysis locations are selected with the aid of a rapid imaging technique, such as an SEM image prepared with backscattered electrons, which are sensitive to compositional variations, or with the associated optical microscope.

Often, more detailed information is needed on the distribution of a constituent. The technique of X-ray area scanning, or *dot mapping*, can provide a qualitative view of elemental distributions. As the beam is scanned in a raster pattern on the specimen, a cathode ray tube scanned in synchronism is used to display a full white dot whenever the X-ray detector (WDS or EDS) detects an X ray within a certain narrow energy range. The pattern of dots is recorded on film to produce the dot map. Dot maps are subject to the following limitations:[4]

1 The information is qualitative in nature. The area density of dots suggests local concentration differences, but the count rate at each point, which is fundamental information required for quantitation, is lost.

2 Because of count rate performance and peak-to-background, WDS is preferable to EDS for mapping, particularly for minor and trace constituents.
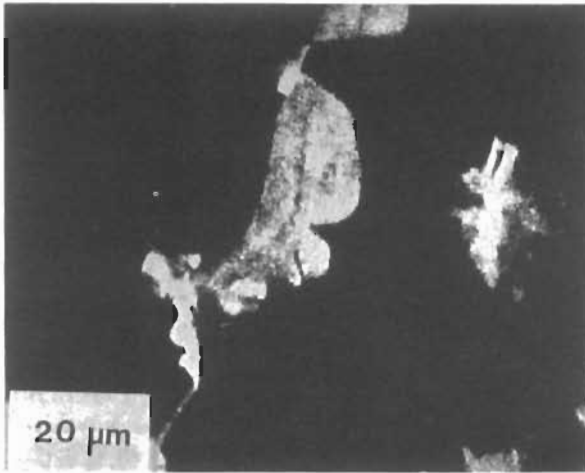
Figure 5   X-ray area scan (dot map) showing the distribution of zinc at the grain boundaries of copper.

3 Mapping of major constituents can be carried out in approximately 15–30 minutes of scanning per image. Minor constituents require 0.5–3 hours, and trace constituents require 3–10 hours. An example of a dot map of zinc at concentrations in copper as low as 1% is shown in Figure 5; 6 hours of scan time was needed to produce a dot map at this level.

4 While low concentrations can be mapped against a background of 0 concentration, as shown in Figure 5, dot mapping has poor contrast sensitivity. It would be difficult to map a 5% concentration modulation above a general level of 50% because there is no provision for subtracting the influence of the dominant general signal.

5 Since no background correction can be made, dot maps of minor and trace constituents are subject to possible artifacts caused by the dependence of the bremsstrahlung on composition, particularly with EDS X-ray measurement.

Quantitative compositional mapping overcomes the limitations of dot mapping by recording in computer memory the count rates for all constituents of interest at all picture elements in the scan.[4] Complete quantitative procedures are then applied to the count rate arrays: dead time correction, background correction, standardization, and matrix correction. The resulting concentration arrays are presented as images on a digital display with a gray or color scale encoding the
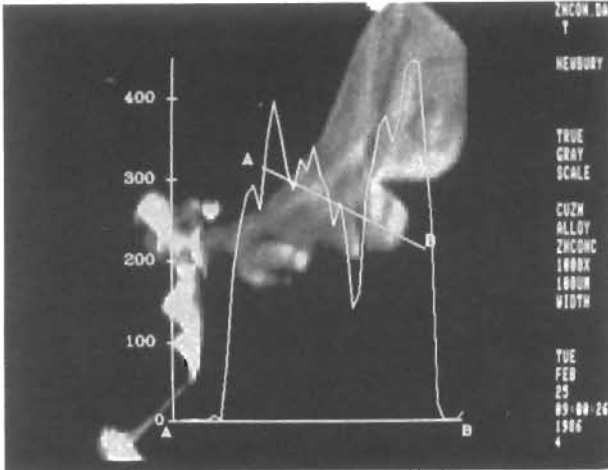
a

b

Figure 6 (a) Quantitative compositional map of the distribution of zinc at the grain boundaries of copper; gray scale corresponds to the concentration range 0–10% wt.; superposed compositional profile (vertical scale, 0–4.0% wt.) along the locus $\overline{AB}$. (b) Contrast enhancement applied to emphasize low-concentration structure (0.1% wt. = 1000 ppm) at arrows; image width 100 μm.

concentration information. Typical dwell times per pixel are 0.1–2 s, which restricts detection limits in imaging to approximately 500 ppm with high beam currents and WDS detection; comparable accuracy to single point analysis can be achieved in the mapping mode. An example is shown in Figure 6a of a digital compositional map of the same area as Figure 5; concentration levels as low as 0.1% wt. are visible. Digital compositional maps can be subjected to subsequent image processing to enhance features of interest. Contrast expansion of Figure 6a, shown in Figure 6b, reveals fine details in the zinc diffusion zone. This combination of images supported by complete numerical concentration values at every pixel, including the measurement statistics, is a powerful tool for solving a wide range of problems.

Conclusions

The electron probe X-ray microanalyzer provides extraordinary power for measuring the elemental composition of solid matter with μm lateral spatial resolution. The spatial resolution, limited by the spread of the beam within the specimen, permits pg samples to be measured selectively, with elemental coverage from boron to the actinides. By incorporating the imaging capability of the SEM, the electron probe X-ray microanalyzer combines morphological and compositional information.

Several future trends are evident. The great utility of true compositional maps suggests that this mode of operation will replace the now antiquated dot maps. Greater use of computer-aided imaging and analysis will increase the efficiency of the instrument in applications where large quantities of data are required. Improved long-term stability will permit the long counting times required for routine application of trace analysis. Continued development of advanced correction methods will address special difficulties raised by complex specimens such as multi-layers and inhomogeneous particles. Lastly, the need for improved lateral and depth spatial resolution will lead to increased application of low beam energy analysis.

Related Articles in the Encyclopedia

EDS, XRF, and SEM

References

1 R. Castaing. *Application of Electron Probes to Local Chemical and Crystallographic Analysis.* Ph.D. thesis, University of Paris, 1951.

2 J. I. Goldstein, D. E. Newbury, P. Echlin, D. C. Joy, C. E. Fiori, and E. Lifshin. *Scanning Electron Microscopy and X-Ray Microanalysis.* Plenum, New York, 1981. References 2 and 3 are comprehensive textbooks covering all

aspects of electron probe microanalysis and the associated technique of scanning electron microscopy.

3 D. E. Newbury, D. C. Joy, P. Echlin, C. E. Fiori, and J. I. Goldstein. *Advanced Scanning Electron Microscopy and X-Ray Microanalysis.* Plenum, New York, 1986.

4 D. E. Newbury, C. E. Fiori, R. B. Marinenko, R. L. Myklebust, C. R. Swyt, and D. S. Bright. Compositional Mapping with the Electron Probe Microanalyzer. *Anal. Chem.* 1990, 62, Part I, 1159A; Part II, 1245A.

5 G. F. Bastin and H. J. M. Heijligers. Quantitative Electron Probe Microanalysis of Ultralight Elements (Boron–Oxygen). Scanning. **12,** 225, 1990.